# Tau and spectraplakins promote synapse formation and maintenance through Jun kinase and neuronal trafficking

André Voelzmann[2], Pilar Okenve-Ramos[1], Yue Qu[2], Monika Chojnowska-Monga[1], Manuela del Caño-Espinel[3], Andreas Prokop[2,4], Natalia Sanchez-Soriano[1,4*]

1) University of Liverpool, Institute of translational Medicine, Department of Cellular and Molecular Physiology, Crown Street, Liverpool, L69 3BX, UK

2) The University of Manchester, Faculty of Life Sciences, Michael Smith Building, Oxford Road, Manchester M13 9PT, UK

3) Instituto de Biología y Genética Molecular-Departamento de Bioquímica y Biología Molecular y Fisiología, Universidad de Valladolid-CSIC, Valladolid, Spain

Running title**:** Tau and Shot regulate synapses via JNK

Key words: *Drosophila*, neurodegeneration, transport, tau, axons, microtubules, synapses

4) shared authors for correspondence:

Natalia Sánchez-Soriano
University of Liverpool
Institute of translational Medicine
Department of Cellular and Molecular Physiology
Crown Street
Liverpool, L69 3BX, UK
n.sanchez-soriano@liverpool.ac.uk

Andreas Prokop
The University of Manchester
Oxford Road
Manchester M13 9PT
Tel: +44-(0)161-27-51556
Fax: +44-(0)161-27-51505
Andreas.Prokop@manchester.ac.uk

**Impact statement (15-30)**

A novel regulatory cascade downstream of Tau and spectraplakins delivers synaptic proteins to axonal terminals in the developing and ageing brain, providing potential explanations for precocious synapse loss in dementias.

## Abstract

The mechanisms regulating synapse numbers during development and ageing are essential for normal brain function and closely linked to brain disorders including dementias. Using *Drosophila*, we demonstrate roles of the microtubule-associated protein Tau in regulating synapse numbers, thus unravelling an important cellular requirement of normal Tau. In this context, we find that Tau displays a strong functional overlap with microtubule-binding spectraplakins, establishing new links between two different neurodegenerative factors. Tau and the spectraplakin Short Stop act upstream of a three-step regulatory cascade ensuring adequate delivery of synaptic proteins. This cascade involves microtubule stability as the initial trigger, JNK signalling as the central mediator, and kinesin-3 mediated axonal transport as the key effector. This cascade acts during development (synapse formation) and ageing (synapse maintenance) alike. Therefore, our findings suggest novel explanations for intellectual disability in Tau deficient individuals, as well as early synapse loss in dementias including Alzheimer's disease.


## Introduction

The correct formation and subsequent maintenance of synapses, is a key prerequisite for brain development, function and longevity. Precocious loss of synapses is observed in late onset neurodegenerative diseases including Alzheimer's disease (AD) and Frontotemporal Dementia (FTD), likely contributing to the cognitive decline and neuronal decay observed in patients (Pooler et al, 2014; Saxena & Caroni, 2007; Serrano-Pozo et al, 2011). Therefore, the characterisation of mechanisms maintaining synapses during ageing would have major implications for our understanding of dementias.

The development of synapses and their maintenance during ageing is dependent on sustained transport of synaptic proteins from the distant soma, driven by motor proteins

which trail along the bundles of microtubules in axons and dendrites (Goldstein et al, 2008). Microtubules are regulated by microtubule binding proteins which are therefore in a key position to regulate synapse formation and maintenance (Prokop, 2013).

Tau is a microtubule associated protein (MAP) discovered in the mid-seventies (Weingarten et al, 1975). Reduction in Tau levels has been linked to intellectual disability (Sapir et al, 2012) and a class of brain disorders termed "dementias which lack distinctive histopathology" (DLDH) (Zhukareva et al, 2001). Tau detachment from MTs is linked to prominent neurodegenerative diseases such as Alzheimer's disease, Frontotemporal Dementia and some forms of Parkinson's disease (Kovacs, 2015). *In vitro*, Tau has the ability to regulate microtubule properties including stability, cross-linkage and polymerisation (Morris et al, 2013). Through such functions, Tau would be expected to regulate multiple aspects of neuronal cell biology, but its physiological roles are still not understood and highly debated (Morris et al, 2013). This might partly be due to experimental challenges posed by functional redundancy, where other MAPs are proposed to mask physiological roles of Tau (Ma et al, 2014; Takei et al, 2000).

A good model in which to deal with functional redundancy is the fruit fly *Drosophila melanogaster*. As is ideal for studies of Tau, *Drosophila* neurons provide access to powerful genetics, they are readily established for research on the neuronal cytoskeleton (Sánchez-Soriano et al, 2010), on neuronal transport (Schwarz, 2013) and on synapses (Prokop & Meinertzhagen, 2006). Importantly, concepts and mechanisms gained from work in flies are often well conserved in higher organisms (Bellen et al, 2010; Jaiswal et al, 2012).

Work in *Drosophila* suggested that the spectraplakin Short stop (Shot), a large actin-MT linker molecules and potent regulators of microtubules, could display potential functional overlap with Tau during microtubule stabilisation (Alves-Silva et al, 2012a; Prokop et al, 2013). This hypothesis is attractive because the well-conserved mammalian spectraplakin Dystonin is already linked to a neurodegenerative disease (type VI hereditary sensory

autonomic neuropathy; OMIM #614653; )(Ferrier et al, 2013), and its paralogue ACF7/MACF1 plays important roles during brain development (Goryunov et al, 2010; Ka & Kim, 2015). Since ACF7 continues to be expressed in the brain, it is tempting to speculate that it might be required for neuronal maintenance (Bernier et al, 2000).

Here we use *Drosophila* neurons, in culture and *in vivo* alike, to demonstrate novel roles of Tau in regulating the formation and maintenance of synapses during ageing, by coordinating the intracellular trafficking of synaptic proteins. Thus, we show that the role of Tau in synapse regulation occurs in functional overlap with Shot. The robust *shot-tau* double-mutant phenotypes enabled us to study the mechanistic cascade composed of three steps: microtubule stability as the trigger, the JNK signalling pathway as the mediator and kinesin-3 mediated axonal transport of synaptic proteins as the key effector. We propose a new mechanism based on the loss of Tau function which could explain intellectual disability in MAPT mutant individuals and precocious synapse loss in tau-related neurodegeneration (Saxena & Caroni, 2007; Serrano-Pozo et al, 2011).

## Results

### Tau is required for the formation of synapses

To study synaptic roles of *Drosophila* Tau, we first used primary *Drosophila* neurons generated from *tau* mutant embryos. Primary fly neurons are genetically and experimentally highly amenable and provide robust cellular and subcellular readouts (Prokop et al, 2012). These cultures are also particularly suited for the study of embryonic lethal mutations since they allow the examination of neurons beyond the embryonic lethal stage. Already 8 hours *in vitro* (HIV), these neurons show transport of synaptic material in the growing axon (Sánchez-Soriano et al, 2010) and after 2 days *in vitro* (DIV), they display functional presynaptic sites (Küppers-Munther et al, 2004; Küppers et al, 2003) that can be reliably stained with antibodies against presynaptic proteins (Figure 1–supplement 1). They contain dense bars

and synaptic vesicle accumulations which undergo excitation-dependent uptake and release (Küppers-Munther et al, 2004; Küppers et al, 2003).

The *Df(3R)tauMR22* mutation ($tau^{MR22}$) is an embryonic lethal chromosome deletion that uncovers most of the *Drosophila tau* gene and is a true null allele (Bolkan & Kretzschmar, 2014; Doerflinger et al, 2003b). We found that $tau^{MR22}$ mutant primary neurons at 2 DIV show a decrease in the number of puncta positive for Bruchpilot (Brp) and Synaptotagmin (Syt) (Bruchpilot/Brp: 42%; Synaptotagmin/Syt: 59%; all compared to wildtype control neurons; Figure 1). Our finding suggest that tau-deficient primary neurons contain fewer Brp and Syt positive presynaptic specialisations. In the following, we will refer to this phenotype as synapse reduction.

To confirm that this reduction in synapses numbers was due to the loss of Tau, we performed rescue experiments using Gal4-induced neuronal expression of *UAS-tau-GFP* (Doerflinger et al, 2003b) in $tau^{MR22}$ mutant neurons. We found a significant improvement of the $tau^{MR22}$ mutant phenotype (Figure 1A-B). We concluded that absence of Tau causes a reduction in presynaptic sites.

Tau displays functional overlap with the spectraplakin Shot

To assess potential functional overlap of Tau with the *Drosophila* spectraplakin Shot, we first analysed $shot^{3}$ mutant primary neurons at 2 DIV. We found a reduction in synapse numbers (Brp: 62%; Syt: 67%; Figure 1C-D), consistent with previous descriptions *in vivo* (Löhr et al, 2002; Prokop et al, 1998). We confirmed that this reduction in synapse numbers was due to the loss of Shot by using Gal4-induced neuronal expression of *UAS-shot-GFP* (Alves-Silva et al, 2012b; Sánchez-Soriano et al, 2009) which significantly rescued the synapse phenotype in $shot^{3}$ mutant neurons (Figure 1-suplement 2), confirming the involvement of Shot.

We then assessed potential functional overlap of Shot and Tau. First, we analysed primary neurons double-mutant for the *shot*$^{3}$ and *tau*$^{MR22}$ null alleles (*shot-tau*) which showed even lower synapse numbers (Brp: 22%; Syt: 39%; Figure 1C-D) than either of the single mutant neurons. Notably, these analyses were performed on clearly polarised neurons with well developed axons to exclude indirect effects caused by defective axon growth (Fig. 3 supplement 3). Despite that, we found that the double-mutant neurons displayed reduced branch numbers (Fig. 3 supplement 3F). However, we could demonstrate that the lower number in branches is not the cause for synapse reduction by using knock-down experiments as well as rescue experiments (explained in detail below, Fig. 3 supplement 3 and Fig. 3 supplement 4, see also Discussion).

In further support of functional overlap also our genetic interaction studies revealed a synapse reduction phenotype in *shot*$^{3/+}$ *tau*$^{MR22/+}$ double heterozygous mutant neurons (Fig.5A). Finally, we performed cross-rescue experiments by expressing a *shot* transgene in *tau*$^{MR22}$ mutant neurons and a *tau* transgene in *shot*$^{3}$ mutant neurons. In both cases, Syt staining revealed a rescue of the synapse reduction phenotype (Figure 1 supplement 3). Taken together, our results indicate that Shot and Tau functionally overlap, rather than act hierarchically in the same pathway.

Next, we investigated synaptic phenotypes *in vivo.* Since *shot*$^{3}$ and *tau*$^{MR22}$ animals are embryonic lethal, we analysed them at late embryonic stage 16, when Syt is already confined to nascent synaptic terminals, as can be reliably imaged at neuromuscular junctions (NMJs; Figure 2 and Figure 2–supplement 1 for a schematic drawings of the embryonic NMJ) (Littleton et al, 1993). In *shot-tau* mutant embryos, Syt levels at NMJs were reduced to 48%, whereas *shot* mutant embryos showed a milder reduction to 71%, and *tau* mutant embryos no detectable effect (Figure 2). Taken together, our data suggest that Tau is required for the formation of synapses in culture and *in vivo,* and that Tau and Shot functionally overlap in this context.

Synapse maintenance in the ageing brain requires Tau and Shot

Tau and Shot remain highly expressed in mature neurons (Figure 6A), and we tested whether they are required also for synapse maintenance. For this, we used the GAL4-UAS system to co-express previously used and validated *UAS*-iRNA constructs for both genes in the same neurons (Bolkan & Kretzschmar, 2014; Subramanian et al, 2003). This strategy takes out Tau and Shot functions with some delay, due to the late onset of GAL4 expression and the persistence of Tau and Shot proteins (Figure 3-supplement 1).

We first used this approach in cultured primary neurons, where combined knock-down of *tau* and *shot* caused no reduction in the number of Syt-labelled presynaptic sites at 3 and 18 DIV as compared to wildtype controls (Figure 3A-B), indicating normal synapse development. However, at 26 DIV, Syt puncta in knock-down neurons were reduced to 41% (Figure 3A-B), which was comparable to the *shot-tau* double-mutant phenotype at 2 DIV (Figure 1). At all time points (i.e. 3, 18 and 26 DIV), there were no measurable changes in axonal length nor in branch number when compared to control neurons (Figure 3–supplement 4 A, B, C and E), clearly indicating that the strong reduction in Syt positive synapses in 26 DIV knock-down neurons was not a secondary effect of morphological changes such as in number of branches and axonal length (Figure 3 A and B).

To assess roles in synapse maintenance also *in vivo* in the ageing brain, we used *atonal-Gal4* (*ato-Gal4*) to drive gene expression in dorsal cluster (DC) neurons of the adult brain (Zschätzsch, 2014) (illustrated in Figure 3-supplement 1). In these experiments, we expressed GFP-tagged Synaptotagmin (Syt-GFP) to label synapses, either alone or together with $shot^{RNAi}$ and/or $tau^{RNAi}$. We compared young flies at 2-5 days after eclosion with old flies at 24-29 days. We found that the number of Syt-GFP labelled synapses in DC neurons decreased to 34% in aged specimens expressing both $shot^{RNAi}$ *and* $tau^{RNAi}$ when normalised to young flies of the same genotype (Figure 3C-D). This age-dependent decrease in

synapse numbers did not occur in control flies (Figure 3C-D), and single knock-down of either *shot* or *tau* only showed a non-significant tendency to lose synapses over time (Figure 3D). Notably, aged double knock-down DC neurons had no reduction in the number of axonal branches (as assessed with the myr-tdTomato membrane marker; Figure 3E-F), indicating that also *in vivo* precocious synapse decay was not due to axonal loss.

From our studies in culture, in embryos and in the adult brain, we conclude that Tau and Shot are required for synapse development during early stages, and for synapse maintenance in ageing neurons, where their combined deficiency causes precocious synapse loss.

Tau and Shot control intracellular trafficking of synaptic proteins

Synapse formation and maintenance require that synaptic proteins synthesised in the soma, are actively transported through the axon towards the distant presynaptic sites. In *Drosophila* primary neurons, transport of endogenous synaptic proteins already starts at 8 hours *in vitro* (HIV) when synaptic proteins appear as dotted patterns along axons and in growth cones (Sánchez-Soriano et al, 2010) (Figure 4A-B). This is similar in rat hippocampal neurons (Bonanomi et al, 2005). Already at this early stage, *shot-tau* double mutant neurons display a strong decrease in synaptic proteins in growth cones and axons (Figure 4A-B), indicating potential intracellular transport defects.

To study intracellular transport, we analysed the dynamics of Syt-GFP using live imaging of neurons at 8 HIV. In *shot-tau* mutant neurons, the percentages of anterograde and retrograde displacements and retrograde velocities of Syt-GFP containing vesicles, were not affected and anterograde velocities were only slightly increased. In contrast, the number of Syt vesicles within the axon showed a sharp decrease to ~40% in *shot-tau* mutant neurons when compared to controls (Figure 4C). Notably, this decrease in axonal vesicles is accompanied by an increase in the number of somatic Syt-GFP puncta to ~159% (Figure

4C). Similarly, also endogenous Syt was increased in somata of *shot-tau* mutant neurons, both in culture and in *in vivo* (Figure 4D-E).

These phenotypes in *shot-tau* mutant neurons suggested aberrant intracellular trafficking of Syt-containing vesicles, potentially due to a road block in the soma.

Tau and Shot regulate the activity of kinesin-3

Type 3 kinesins are the predominant motors driving axonal transport of synaptic proteins (Hirokawa et al, 2010). This is also the case for the *Drosophila* homologue Unc-104 (also called Imac) (Pack-Chung et al, 2007). We found that *unc-104*$^{170}$ null mutant primary neurons at 2 DIV have a vast reduction of Syt-stained synapses (Figure 5A). This phenotype is strikingly similar to the one observed in *shot-tau* mutant neurons, and suggested that Shot-Tau might regulate Unc-104 function.

To test this hypothesis, we performed genetic interaction studies. We found that primary neurons stained for Syt at 2 DIV and heterozygous for all of the three genes (*shot*$^{-/+}$ *unc-104*$^{-/+}$ *tau*$^{-/+}$) displayed significant reduction in the number of Syt-stained synapses when compared to heterozygous condition of the *unc-104* or *shot-tau* mutant alleles alone (Figure 5A). Also triple-heterozygous mutant embryos at late stage 16 displayed reduced Syt staining at neuromuscular terminals, but increased staining in the cell bodies of CNS and sensory neurons (Figure 5C; see Figure 2 supplement 1 for a schematic drawing of the embryonic NMJ and CNS). Therefore, *unc-104*$^{170}$ mutant, *shot-tau* mutant, and triple-heterozygous mutant neurons all show a similar phenotypes, both in culture and *in vivo*, suggesting a functional link between these three proteins.

Type 3 kinesins are anterograde motor proteins that move towards axon tips in mouse neurons (Niwa et al, 2013), and we also find *Drosophila* Unc-104 to be distally enriched in the axons of primary neurons at 2 DIV and in embryonic motorneurons *in vivo* (Fig. 5D-E). In

mouse, this distal localisation was shown to be suppressed when blocking kinesin-3 mobility (Niwa et al, 2013). Also in *shot-tau* mutant neurons in culture and *in vivo*, Unc-104 localisation in distal axons is reduced whereas levels in the somata are increased (Figure 5D-E), suggesting that insufficient amounts of Unc-104 move from the somata into axons.

To test whether diminished Unc-104 levels in axons are the cause for the synaptic defects in *shot-tau* mutant conditions, we over-expressed Unc-104, which fully restored synapse numbers in *shot-tau* mutant neurons at 2 DIV (Figures 5B *versus* 1D). Notably, Unc-104 over-expression in *shot-tau* mutant neurons achieves this rescue of synapses in neurons with significantly less axonal branches (Figure 3 supplement 2F), clearly demonstrating that both features are regulated independently of each other.

We next examined whether Unc-104 plays comparable roles also during synapse maintenance in the ageing brain. We used the *ato-Gal4* driver (Zschätzsch, 2014) and co-expressed Unc-104 together with $shot^{RNAi}$ and $tau^{RNAi}$. To label synapses we expressed the presynaptic marker neuronal Synaptobrevin-GFP (nSyb-GFP), due to technical reasons the use of nSyb-GFP was more convenient than Syt-GFP. Consistent with our previous findings with Syt-GFP (Figure 3C-D), also nSyb-GFP revealed age-dependent synapse reduction upon $shot^{RNAi}$ and $tau^{RNAi}$ expression, clearly confirming our previous data (Figures 5 supplement 2 and 8E-F). When Unc-104 was co-expressed, synapse reduction was clearly rescued (Figure 5 supplement-2).

Taken together, our data are consistent with a model where Shot-Tau loss generates a road block which inhibits Unc-104 translocation from the soma into axons causing synaptic defects at developmental stages and in ageing neurons.

<u>Loss of Shot-Tau induces microtubule destabilisation accompanied by changes in JNK activation</u>

To address the mechanistic links from loss of Shot-Tau to aberrant transport and synaptic defects, we focussed on microtubules. Shot localises along microtubules, and *shot* mutant neurons treated with the microtubule-destabilising drug nocodazole display unusual gaps in their axonal microtubule bundles (Figure 6B-C) (Alves-Silva et al, 2012b; Sánchez-Soriano et al, 2009). Tau also localises along microtubules (Figure 6A, Supplementary video 1), and $tau^{MR22}$ mutant neurons likewise displayed axonal microtubule gaps upon nocodazole treatment which could be rescued with targeted expression of Tau (Figure 6B-C). Both, *shot* or *tau* mutant neurons treated with nocodazole, displayed on average one gap per axon. This number is significantly increased to ~3 gaps in *shot-tau* mutant neurons (Figure 6B-C), demonstrating that Tau and Shot share a common function in microtubule stabilisation.

To test whether their roles in microtubule stabilisation and synapse regulation are linked, we treated *shot-tau* mutant embryos at early stage 16 for 3 hrs with the microtubule-stabilising drug epothilone B (Goodin et al, 2004). We found a significant rescue of Syt levels at motoraxonal endings, which was not observed in vehicle-treated controls (Figure 6D-E). Therefore, a decrease in microtubule stability is a likely cause for defective transport of synaptic proteins in *shot-tau* mutant neurons. It could be argued that Shot-Tau dependent microtubule stabilisation directly regulates processive advance of kinesins in axons (see Discussion), yet the rather normal transport dynamics we observed upon live imaging in *shot-tau* mutant neurons clearly excluded this possibility (Figure 4C).

Instead, we hypothesised that microtubule aberration indirectly promotes a transport roadblock in somata. As a potential mediator, we suspected the JNK signalling pathway which is known to respond to a number of cellular stresses (see Discussion). To test our hypothesis, we investigated the pattern of JNK activity, using an antibody against phosphorylated JNK (JNK-P) (Langen et al, 2013). In wild type embryos at stage 16, we found high accumulations of JNK-P at motoraxon tips and low levels in the somata of CNS and sensory neurons (Figure 6F and 7A), i.e. a localisation pattern similar to that of synaptic

proteins and Unc-104 (Figure 5C-E). This distribution was altered in single *tau*$^{MR22}$ or *shot* $^{3}$ mutant embryos, showing higher levels of JNK-P in neuronal somata and lower levels at the tips of motoraxons (Figure 7A). This altered pattern was intensified in *shot-tau* double mutant neurons (Figure 7A) and clearly reminiscent of the redistribution patterns observed with synaptic proteins and Unc-104 in these neurons (Figure 4E and 5E). Notably, these changes in the pattern of JNK activation were reproduced when inducing microtubule stress by applying nocodazole to early stage 16 wildtype embryos (Figure 6F). Complementary to this finding, treatment of *shot-tau* mutant neurons with the microtubule stabilising drug epothilone B, increased the localisation of JNK-P at axonal tips and reduced the aberrant localisation in somata (Figure 6 supplement 1A, B).

These data suggested a cascade of events where *shot-tau* mediated microtubule destabilisation or stress triggers abnormal JNK activation in somata which, in turn, causes a somatic block of Unc-104 mediated synaptic transport. In strong support of this hypothesis, the three key players of this cascade, JNK-P, Unc-104 and synaptic proteins, show a striking correlation by concentrating unanimously at axon tips in wildtype, but in somata in *shot-tau* mutant neurons (Figure 4E, 5E and 7A).

<u>Aberrant JNK signalling upon Shot-Tau loss causes the somatic road-block of Kinesin-3 transport and synaptic defects</u>

To prove that JNK acts downstream of *shot-tau* to regulate Unc-104, we first expressed a constitutively active variant of the MAPKK Hemipterous (Hep$^{AC}$), a known activator of the JNK pathway (Glise et al, 1995). In late stage 16 embryos, indiscriminate JNK activation through Hep$^{AC}$ triggered an accumulation of Unc-104 and Syt in somata and a decrease of both proteins at axon tips (Figure 7B-C). Also in primary mature neurons at 2 DIV, Hep$^{AC}$ caused a reduction in the number of synapses to 43% (Figure 8A-B). Therefore, Hep$^{AC}$ expression mimicked the defects observed in *shot-tau* mutant neurons, consistent with a

model where aberrant JNK pathway activation upon Shot-Tau loss causes the somatic block of Unc-104-dependent synaptic transport.

If our model is correct, attenuation of the JNK pathway should rescue the synaptic defects in *shot-tau* mutant neurons. To downregulate the JNK pathway, we used loss-of-function of the JNK activating kinase Wallenda/DLK (*wnd*$^{2}$) (Valakh et al, 2013) and overexpression of the JNK inhibiting phosphatase Puckered (Puc) (Martín-Blanco et al, 1998). When combined with the *tau*$^{MR22}$ mutation, both genetic tools for JNK downregulation fully rescued the synaptic defects in primary neurons at 2 DIV (figure 8A-B). Even more, *wnd*$^{2}$ fully rescued synapse reduction in *shot-tau* double mutant neurons at 2 DIV (figure 8A-B), and Syt levels at NMJs of *shot-tau* mutant embryos *in vivo* (Figure 8C-D *versus* Figure 2).

So far, our data suggest that JNK acts downstream of *shot-tau* to regulate Unc-104. In this case, attenuation of the JNK pathway should also rescue aberrant Unc-104 localisation in *shot-tau* mutant neurons. Accordingly, *wnd*$^{2}$ restored correct localisation of Unc-104 in *shot-tau* double mutant neurons at 2 DIV (figure 8 supplement 1), and in *shot-tau* mutant embryos *in vivo* (figure 8 supplement 2 B *versus* Figure 5 D, E).

Having confirmed JNK as the essential mediator of *shot-tau* synaptic defects, we tested whether it acts through the canonical pathway involving the AP1 transcription factor (Ciapponi & Bohmann, 2002), or by phosphorylating other targets in the cytoplasm. For this, we used a well established LOF mutant allele of the *kayak/c-fos* gene (*kay*$^{2}$) which removes one constituent of the AP1 heterodimer and mimics various known JNK mutant phenotypes (Ciapponi & Bohmann, 2002). Unlike *wnd*$^{2}$ or Puc overexpression, the *kay*$^{2}$ mutation failed to rescue the synaptic phenotypes of *tau*$^{MR22}$ in primary neurons (Figure 8A-B). This strongly suggests that the JNK pathway inhibits synaptic transport by acting independently of AP-1 dependent transcription.

In conclusion, the JNK pathway is both required and sufficient to mediate between Shot-Tau loss and their downstream synaptic phenotypes in developing neurons by causing a

transport roadblock, and this likely occurs through phosphorylating cytoplasmic targets in the soma.

JNK mediates ageing related synaptic decay caused by Shot-Tau loss

To test whether JNK plays comparable roles also during synapse maintenance in the ageing brain, we used the *ato-Gal4* driver (Zschätzsch, 2014) and co-expressed a dominant negative variant of the *Drosophila* JNK homolog Basket ($bsk^{DN}$) (Adachi-Yamada et al, 1999) together with $shot^{RNAi}$, $tau^{RNAi}$ and nSyb-GFP. We found that co-expression of $bsk^{DN}$ was able to rescue the synapse reduction phenotype (Figure 8E, F), thus confirming JNK as a mediator between the effects of *shot-tau* and precocious synapse decay also in ageing neurons.

## Discussion

A new mechanism of synaptic pathology caused by loss of Tau and Shot

The aim of our studies was to understand the role of endogenous Tau in neurons with particular attention to synapses. This effort was essentially aided by our finding that Tau and Shot are functionally redundant, and the subsequent incorporation of Shot into our studies. The robust phenotypes of *shot-tau* double-mutant neurons enabled us to demonstrate roles of Shot-Tau during the formation and maintenance of pre-synaptic sites in axons, and unravel the underlying mechanistic cascade which involves three major steps. Firstly, the absence of Shot-Tau causes microtubule destabilisation. Secondly, this cytoskeletal stress causes aberrant JNK activity patterns with upregulation in somata and downregulation at axon tips. Thirdly, aberrant JNK activation leads to a somatic roadblock for kinesin-3 mediated transport, thus inhibiting the delivery of synaptic proteins and eventually causing synapse loss. Depending on whether the functions of Tau and/or Shot are removed during

development or ageing, either the formation or the maintenance of synapses are affected, respectively

Our model explaining the function of Tau and Shot in synapses establishment and maintenance, by regulating intracellular transport is supported by loss- and gain-of-function experiments, genetic interactions and cross-rescue experiments. The initial finding that *shot-tau* mutant neurons had reduced branch numbers, could have suggested that defects on synapse numbers is indirect. However, experiments with double knock-down in culture and in the adult brain clearly showed strong synapse reduction whilst maintaining normal branch patterns, and Unc-104 rescued synapse reduction in *shot-tau* mutant neurons without major increases of the branch pattern in these neurons. These results clearly demonstrate that changes in neuronal morphology are not the cause of changes in synapse number.

Notably, the synaptic function of Tau described here for *Drosophila* might be conserved in higher animals or humans, since also aged Tau knock-out mice develop a reduction of synaptic proteins from the hippocampus (Ma et al, 2014).

Implications of our findings for Tau-related pathologies

Our findings provide potential new mechanistic explanations for various tau related brain disorders. For example, microdeletions in the region of MAPT (the human tau gene) cause intellectual disability (Sapir et al, 2012), and Tau's synapse-promoting roles may well contribute to this pathology. Furthermore, various tauopathies are characterised by precocious pathological loss of synapses, our data suggest that loss of tau could lead to defective synapse maintenance and eventually synapse loss. For example, a prominent group of dementias which lacks distinctive histopathology (DLDH) are characterised by the loss of Tau (Zhukareva et al, 2001). Further tauopathies including Alzheimer disease, typically involve hyper-phosphorylation and aggregate formation of Tau (Hernandez & Avila, 2007; Williams, 2006). In this scenario, there are two parallel, non-exclusive modalities

through which Tau can cause pathology. Firstly, detached hyper-phosphorylated tau attains gain-of-function roles in the cytoplasm damaging neurons through a number of mechanisms (Morris et al, 2013). Secondly, hyper-phosphorylation of tau causes a loss-of-function condition by depleting Tau from microtubules. However, since Tau knock-out mouse models mostly failed to show significant phenotypes and the neuronal functions of endogenous tau remain little understood, the pathological importance of Tau loss from microtubules has been marginalised (Morris et al, 2013). Our results now re-emphasise the notion that loss of Tau from microtubules could contribute to neurodegenerative pathology and deliver mechanistic explanations.

To unravel pathomechanisms caused by the loss of Tau, we mostly used combined depletion of Shot and Tau, which gave us strong phenotypes, ideal for short-term experimental approaches. However, we found similar, yet milder phenotypes if only Tau was depleted, suggesting that the mechanisms described here could well contribute to slow disease progression in tauopathies. Our discovery that spectraplakins are MAPs which functionally overlap with Tau, opens up new experimental avenues for Tau studies. So far, spectraplakins have been linked to the degeneration of sensory and autonomous neurons (Edvardson et al, 2012; Ferrier et al, 2013), and it remains to be elucidated whether they may have similar roles also in the brain. Our results clearly hint at this possibility.

A novel mechanism for Tau-dependent regulation of neuronal transport

The loss of Tau and/or Shot inhibits kinesin-3 mediated transport leading to accumulation of synaptic proteins in the soma of neurons. We propose a road-block mechanism suppressing the initiation of axonal transport in somata of Shot-Tau depleted neurons, which is caused indirectly through microtubule stress and mediated by JNK (Fig. 4B).

The involvement of microtubules in causing a transport block is supported by our experiments using microtubule stabilising and de-stabilising drugs which rescued or mimicked the *shot-tau* mutant phenotypes, respectively. Similarly, axonal transport defects and cognitive deficits of *PS19Tg* mice (expressing the P301S mutant form of human tau) and various other mouse and fly tauopathy models were shown to be rescued by microtubule-stabilising drugs (Gozes, 2011; Quraishe et al, 2013; Shemesh & Spira, 2011; Zhang et al, 2012), suggesting that the mechanisms we described may be conserved and relevant to disease.

The somatic road-block is a novel mechanism through which the loss of Tau can interfere with the transport of synaptic proteins and provides potential explanations also for somatic accumulations of postsynaptic proteins such as PSD-95, AMPA and NMDA receptors observed in mouse tauopathy models (Hoover et al, 2010; Shao et al, 2011). A likely mechanism causing a roadblock in intracellular transport could be the direct inactivation of Unc-104 or its associated adaptor proteins, for example through JNK or other kinases within its pathway. This mode of regulation has a clear precedent in kinesin-1 and its adaptor Jip which are directly phosphorylated by JNK leading to transport inhibition (Edwards et al; Stagi et al, 2006). Unfortunately, our extensive attempts to co-immunoprecipitate JNK and Kinesin-3 were unsuccessful (data not shown), leaving open for now the exact molecular mechanism.

<u>JNK is an important mediator between *shot-tau* induced microtubule stress and synapse loss</u>

We propose that aberrant JNK activation downstream of microtubule destabilisation or stress is the ultimate cause for the defective delivery of synaptic proteins in Tau and/or Shot loss of function. Also in mouse, microtubule stress leads to somatic activation of the JNK pathway, suggesting this mechanism is likely to be conserved with vertebrates (Valakh et al, 2015a).

The JNK pathway is emerging as a central player in neurodegenerative diseases. Its activation is prompted by various neurodegeneration risk factors including oxidative stress, inflammation, and ageing (Lotharius et al, 2005; Valakh et al, 2015b). Furthermore, JNK is activated in AD patients (Coffey, 2014) and in several AD models where it triggers progression of the pathology (Sclip et al, 2014). The new link between Tau/spectraplakins, JNK and synapses we propose here, is therefore likely to provide mechanistic explanations for synaptic pathology observed in AD and other tauopathies.

## Conclusions

We have delivered an important conceptual advance by revealing a new mechanistic cascade which can explain synaptic decay as the consequence of Tau loss from microtubules. Furthermore, we identified a previously unknown functional redundancy with spectraplakins as a promising new avenue for research on Tau. Our findings emphasise that Tau detachment from microtubules can be an important aspect contributing to the pathology of tauopathies in parallel to roles of hyper-phosphorylated Tau in the cytoplasm. Synaptic decay, axonal transport and alterations in the JNK pathway are emerging as central players in a wider range of adult-onset neurodegenerative diseases, and here we have aligned these factors into a concrete mechanistic cascade.

# Materials and methods

## Fly stocks

The following fly stocks were used: the Gal4 driver lines *sca-Gal4* (Sánchez-Soriano et al, 2010), *elav-Gal4* (3rd chromosome) (Luo et al, 1994) and *ato-Gal4* (Zschätzsch, 2014); the mutant alleles *Df(3R)tauMR22* (Bolkan & Kretzschmar, 2014; Doerflinger et al, 2003b), *shot*$^{3}$ (Kolodziej et al, 1995), *unc-104*$^{imac170}$ (courtesy of Dr. T. Schwarz) (Pack-Chung et al, 2007), *wnd*$^{2}$ (Collins et al, 2006) and *kay*$^{2}$ (Ciapponi & Bohmann, 2002) (the latter two courtesy of

S. Sweeney); the UAS lines UAS-*tau-GFP* (Doerflinger et al, 2003a), UAS-*shot-GFP* (Alves-Silva et al, 2012b; Sánchez-Soriano et al, 2009). *tau*$^{GD25023}$ (UAS-tau$^{RNAi}$; Vienna *Drosophila* RNAi Center, Austria) (Bolkan & Kretzschmar, 2014), UAS-shot$^{RNAi}$ (Subramanian et al, 2003), UAS-syt-*GFP* (3$^{rd}$ and 2$^{nd}$ chromosome, Bloomington Stock Center), UAS-*nSyb-GFP* (Bloomington Stock Center), UAS-*tdTomato* (Zschätzsch, 2014), UAS-*Hep-ac* (Glise et al, 1995), UAS-*bsk*$^{DN}$ (Adachi-Yamada et al, 1999) and UAS-*puc* (Martín-Blanco et al, 1998) (the latter five fly stocks courtesy of B. Hassan). Lethal fly stocks were kept over balancers carrying *twist-Gal4* and *UAS-GFP* constructs (Halfon et al, 2002), and combinations of mutant alleles and transgenic constructs were generated using conventional genetic crosses (Roote & Prokop, 2013).

Cell culture

The generation of primary neuronal cell cultures was described previously (Prokop et al, 2012; Sánchez-Soriano et al, 2010). In brief, to generate *Drosophila* primary cultures, neurons were extracted from stage 11 embryos (Campos-Ortega & Hartenstein, 1997). Whole embryos were treated for 1 min with bleach to remove the chorion, sterilized for ~30 s in 70% ethanol, washed in sterile Schneider's/FCS, and eventually homogenized with micro-pestles in 1.5ml tubes containing about 21 embryos per 100 µl dispersion medium. This was followed by 4-5 min incubation in dispersion buffer containing collagenase and dispase at 37°C, followed by a wash in sterile Schneider's/FCS and eventually resuspension in the final volume of Schneider's medium. Cells were plated onto coverslips coated with 0.5 mg/ml Concanavalin A (Sigma) and kept as hanging drop cultures in air-tight special culture chambers (Küppers-Munther et al, 2004) usually for 8 h, 2-3, 18 or 26 days at 26°C. Dilutions of the MT destabilising drug nocodazole (20 uM; Sigma) in Schneider's medium were prepared from stock solutions in DMSO. For controls, equivalent concentrations of DMSO were diluted in Schneider's medium.

Drug treatment of *Drosophila* embryos

Stage 16 embryos were dissected flat in Dulbecco's Phosphate Buffered Saline (Budnik et al, 2006) and cultured for several hours in Schneider's medium with or without drugs. Dilutions of the microtubule destabilising drug nocodazole (20 µM; Sigma) and the microtubule stabilizer epothilone B (50 nM; Sigma) in Schneider's medium were prepared from stock solutions in DMSO. For controls, equivalent concentrations of DMSO were diluted in Schneider's medium.

Immunohistochemistry

Primary fly neurons were fixed in 4% paraformaldehyde (PFA) in 0.1 M phosphate buffer (PB; pH 7–7.2) for 30 min at room temperature (RT). Stage 16 embryos were dissected flat in Dulbecco's Phosphate Buffered Saline (Budnik et al, 2006) and fixed with 4% PFA for 30 min. Adult fly brains were dissected in Dulbecco's Phosphate Buffered Saline and fixed with 4% PFA for 15 min. Antibody staining and washes were performed with Phosphate Buffered Saline supplemented with 0.3% Triton X-100. Staining reagents: anti-tubulin (clone DM1A, mouse, Sigma; alternatively, clone YL1/2, rat, , Millipore Bioscience Research Reagents); anti-FasII (clone ID4, mouse, DSHB, RRID: AB_532376); anti-GFP (goat, Abcam RRID: AB_305643); Cy3/FITC-conjugated anti-HRP (goat, Jackson ImmunoResearch); anti-Syn (SYNORF1 3C11, mouse, DSHB, RRID:AB_528479); anti-Brp (DSHB, RRID:AB_2314867); anti-Syt (rabbit, was a gift from Dr. S. Sweeney); anti-nSyb and anti-Unc104 (both rabbit, were a gift of Dr. T. Schwarz); anti-Elav (rat, DSHB, RRID:AB_528218); anti-pJNK (rabbit, pTPpY, Promega, RRID:AB_430864), anti-CD2 (mouse, AbD Serotec, RRID:AB_566608), anti-dTau (Nick Lowe), anti-Shot (Talila Volk) FITC-, Cy3- or Cy5-conjugated secondary antibodies (donkey, purified, Jackson ImmunoResearch). Specimens were embedded in Vectashield.

Microscopy and data analysis

Standard documentation was performed with AxioCam monochrome digital cameras (Carl Zeiss Ltd.) mounted on BX50WI or BX51 Olympus compound fluorescent microscopes. Z-stacks of embryonic CNSs were taken with a Leica DM6000 B microscope and extracted with Leica MM AF Premier software. Z-stacks of adult fly brains were taken with a Leica DM6000 B microscope or with a 3i Marianas Spinning Disk Confocal Microscope. Using custom software written in Python and NumPy, fly brains images taken with a Leica DM6000 B microscope were individually band-pass filtered (A trous wavelet [1][2], linear 3x3 filter, keeping scales 1-4) to remove stationary background.

To quantify the number of synaptic densities in mature neurons in culture and the number of vesicles containing synaptic proteins in 8h neurons in culture, we used ImageJ (RRID:SCR_003070). In detail, we used thresholding to select synaptic densities from axons of single isolated cells, follow by particle analysis. For all experiments done in parallel identical thresholds were used. For the quantification of synapses in mature neurons in culture, we selected polarised neurons with a clear distinguishable axon, the same neurons were used to study axon length and number of branches.

To quantify synaptic proteins or Unc-104 in the soma of neurons we manually selected the area of the somata using the tubulin or HRP channel and measured the signal intensity derived from the Syt or Unc-104 channel. To measure the levels of Unc-104 at the tip of axons we selected an area of the same size at the most distal part of axons and measured the signal intensity derived from the Unc-104 channel. To quantify synaptic proteins at the tip of embryonic motorneurons *in vivo* we manually selected the area occupied by the growth cones using the FasII staining and measured the signal intensity derived from the Syt channel; the background intensity was subtracted. Images used for these measurements did not contain saturated levels. Also to measure the number of synaptic densities in DC neurons in the medulla of the adult brain we used thresholding to select synaptic densities follow by particle analysis. The number of branches in the medulla per DC neuron was

quantified manually. To quantify MT stability upon nocodazole-treatment, we counted the number of breaks in the microtubule bundle per axon.

Time lapse imaging of cultured primary neurons (in Schneider's/FCS) was performed on a Delta Vision RT (Applied Precision) restoration microscope using a 100x/1.3 Ph3 Uplan FI objective and the Sedat filter set (Chroma 89000). The images were collected using a Coolsnap HQ (Photometrics) camera. The temperature control was set to 26°C. For time lapse recording, images were taken every 2 s for 2 min. To generate transport measurements, vesicles containing fluorescently tagged Syt were tracked manually using the manual tracking plugin for ImageJ.

Statistics, replicates and sample-size

All data are shown as mean with SEM. Statistical analyses were performed in GraphPad Prism using Mann-Whitney Rank Sum Tests (indicated as $P_{MW}$) or $Chi^2$ ($P_{Chi}$), with 95% confidence intervals. The exact p-values and sample size are indicated in the figure legends.

For each primary neuronal cell culture experiment (technical replication), approximately 30 to 40 embryos were used. Neurons obtain from those embryos were divided and cultured in 3 to 4 independent chambers (biological replication). The sample size provided corresponds to the number or neurons studied. Most experiments were performed at least 2 times (2 technical repeats) meaning a minimum of 60 embryos were used, and a minimum of 6 independent culture chambers were studied. These experiments are shown in Figure 1B (*tau*$^{-/-}$, 4 technical replications, 11 biological replications), Figure 1D (Syt, *shot*$^{-/-}$, 3 technical replications, 9 biological replications; *shot*$^{-/-}$ *tau*$^{-/-}$, 3 technical replications, 9 biological replications), Figure 1D (Brp *shot*$^{-/-}$, 2 technical replications, 8 biological replications; tau$^{-/-}$ 2 technical replications, 6 biological replications), Figure 3B (all genotypes at each time point 2

technical replications, 6-8 biological replications), Figure 4D (all genotypes 2 technical replications, 6 biological replications), Figure 5B (2 technical replications, 6 biological replications), Figure 8B (*tau*$^{-/-}$ *Uas-Puc*, 3 technical replications, 8 biological repeats; *tau*$^{-/-}$ *wnd*$^{-/-}$, 2 technical replications, 6 biological repeats; *shot*$^{-/-}$ *tau*$^{-/-}$ *wnd*$^{-/-}$, 2 technical replications, 6 biological replications). Other experiments were as follows: *UAS-tau* rescue experiment of synaptic defects (Figure 1B) and microtubule stability defects (Figure 6C) in *tau*$^{-/-}$ were performed with 1 technical replication which included at least 30 embryos distributed in 4 and 2 independent chambers or biological replications, respectively. However, for these particular experiments we used a co-culture technique in which *tau*$^{-/-}$ control neurons were cultured alongside with *tau*$^{-/-}$ UAS-Tau neurons and therefore are subject to the same environmental variations. For *shot-tau* mutant neurons stained with Brp (Figure 1D) we used 1 technical replication which included at least 30 embryos and 3 independent biological replications. For *tau*$^{-/-}$ *kay*$^{-/-}$ and *kay*$^{-/-}$ (Figure 8B), we used 1 technical replication which included at least 30 embryos and 5 independent biological replications. For the measurement of Syt and Syb synaptic puncta in 8 HIV neurons (Figure 4B), we performed 1 technical replication for each synaptic protein, which included at least 30 embryos each and 2 independent biological replications. For the measurement of Unc-104 in 2 day neurons (Figure 5D) we performed 1 technical replication which included at least 30 embryos and 45 neurons were measured. To account for variations in the immunohistochemistry procedure, we calculated the ratio between distal axon and soma.

For the quantification of axonal transport (Figure 4C), we performed 2 technical replications which included at least 30 embryos each, 2 independent biological replications from which 10-14 neurons were analysed.For measurements of Syt in the nascent embryonic NMJ (Figure 2B and 8C) we used at least 15 embryos per genotype (biological replication) and performed at least 2 technical replications. Both controls and mutant embryos were dissected and stained in the same chamber and therefore subjected to equal conditions (Figure 2B shot$^{-/-}$ 3 technical replications, 30 biological replications, tau$^{-/-}$ 2 technical

replications, 15 biological replications, shot$^{-/-}$ tau$^{-/-}$ 3 technical replications, 17 biological replications. Figure 8C shot$^{-/-}$ tau$^{-/-}$wnd$^{-/-}$ 2 technical replications, and 15 biological replications). For treatment of embryos with epothilone B (Figure 6E) we used at least 12 embryos per genotype and performed 2 technical replications. Both controls and shot-tau mutant embryos were present in the same treatment chambers and therefore subjected to equal conditions. For the quantification of Syt in the nascent embryonic NMJ of

For the study of synaptic phenotypes in adult brains (Figure 3D) we performed at least 3 technical replications and used a minimum of 30 brains in total per genotype. For the quantification of axonal branches in adult brains we performed at least 2 technical replications and we used a minimum of 11 brains. For rescues of synaptic phenotypes in adult brains with UAS-*bsk*$^{DN}$ (Figure 8F) we performed 3 technical replications and used a minimum of 40 brains in total.

**Acknowledgements**

This work was made possible through funding by the BBSRC (BB/M007456/1) to N.S.S, by the BBSRC (BB/I002448/1) and Wellcome Trust ISSF (105610/Z/14/Z) to A.P, and the German Science Foundation (DFG; VO 2071/1-1) to A.V. The Bioimaging Facility microscopes used in this study were purchased with grants from the BBSRC, The Wellcome Trust and the University of Manchester Strategic Fund, and the Manchester Fly Facility where flies were kept and genetic crosses performed has been supported by funds from The University of Manchester and the Wellcome Trust (087742/Z/08/Z). We thank Meredith Lees and Egor Zindy for experimental help, Bassem Hassan, Roland Brandt and Nigel Hooper for helpful comments on the manuscript, Thomas Schwarz, Sean Sweeney,Bassem Hassan, Nick Lowe and Talila Volk for kindly providing reagents. Stocks obtained from the Bloomington *Drosophila* Stock Center (NIH P40OD018537) were used in this study.

## Competing interests

The authors declare that there are no competing interests.

## References


Adachi-Yamada T, Nakamura M, Irie K, Tomoyasu Y, Sano Y, Mori E, Goto S, Ueno N, Nishida Y, Matsumoto K (1999) p38 Mitogen-Activated Protein Kinase Can Be Involved in Transforming Growth Factor β Superfamily Signal Transduction in Drosophila Wing Morphogenesis. *Molecular and Cellular Biology* **19:** 2322-2329

Alves-Silva J, Sánchez-Soriano N, Beaven R, Klein M, Parkin J, Millard T, Bellen H, Venken KJT, Ballestrem C, Kammerer RA, Prokop A (2012a) Spectraplakins promote microtubule-mediated axonal growth by functioning as structural microtubule-associated proteins and EB1-dependent +TIPs (Tip Interacting Proteins). *J Neurosci* **32:** 9143-9158

Alves-Silva J, Sanchez-Soriano N, Beaven R, Klein M, Parkin J, Millard TH, Bellen HJ, Venken KJT, Ballestrem C, Kammerer RA, Prokop A (2012b) Spectraplakins Promote Microtubule-Mediated Axonal Growth by Functioning As Structural Microtubule-Associated Proteins and EB1-Dependent +TIPs (Tip Interacting Proteins). *The Journal of Neuroscience* **32:** 9143-9158

Bellen HJ, Tong C, Tsuda H (2010) 100 years of *Drosophila* research and its impact on vertebrate neuroscience: a history lesson for the future. *Nat Rev Neurosci* **11:** 514-522

Bernier G, Pool M, Kilcup M, Alfoldi J, De Repentigny Y, Kothary R (2000) Acf7 (MACF) is an actin and microtubule linker protein whose expression predominates in neural, muscle, and lung development. *Dev Dyn* **219:** 216-225

Bolkan BJ, Kretzschmar D (2014) Loss of tau results in defects in photoreceptor development and progressive neuronal degeneration in Drosophila. *Developmental Neurobiology* **74:** 1210-1225

Bonanomi D, Menegon A, Miccio A, Ferrari G, Corradi A, Kao HT, Benfenati F, Valtorta F (2005) Phosphorylation of synapsin I by cAMP-dependent protein kinase controls synaptic vesicle dynamics in developing neurons. *J Neurosci* **25:** 7299-7308

Budnik V, Gorczyca M, Prokop A (2006) Selected methods for the anatomical study of *Drosophila* embryonic and larval neuromuscular junctions. In *The fly neuromuscular junction: structure and function - Int. Rev. Neurobiol.*, Budnik V, Ruiz-Cañada C (eds), Vol. 75, pp 323-374. San Diego: Elsevier Academic Press

Campos-Ortega JA, Hartenstein V (1997) *The embryonic development of Drosophila melanogaster*, Berlin: Springer Verlag.

Ciapponi L, Bohmann D (2002) An essential function of AP-1 heterodimers in Drosophila development. *Mechanisms of Development* **115:** 35-40

Coffey ET (2014) Nuclear and cytosolic JNK signalling in neurons. *Nat Rev Neurosci* **15:** 285-299

Collins CA, Wairkar YP, Johnson SL, DiAntonio A (2006) Highwire Restrains Synaptic Growth by Attenuating a MAP Kinase Signal. *Neuron* **51:** 57-69

Doerflinger H, Benton R, Shulman JM, Johnston DS (2003a) The role of PAR-1 in regulating the polarised microtubule cytoskeleton in the Drosophila follicular epithelium. *Development* **130:** 3965-3975

688 Doerflinger H, Benton R, Shulman JM, St Johnston D (2003b) The role of PAR-1 in regulating the
689 polarised microtubule cytoskeleton in the *Drosophila* follicular epithelium. *Development* **130:** 3965-
690 3975

691 Edvardson S, Cinnamon Y, Jalas C, Shaag A, Maayan C, Axelrod FB, Elpeleg O (2012) Hereditary
692 sensory autonomic neuropathy caused by a mutation in dystonin. *Ann Neurol* **71:** 569-572

693 Edwards SL, Yu S-c, Hoover CM, Phillips BC, Richmond JE, Miller KG (2013) An Organelle
694 Gatekeeper Function for Caenorhabditis elegans UNC-16 (JIP3) at the Axon Initial Segment.
695 *Genetics* **194:** 143-161

696 Ferrier A, Boyer JG, Kothary R (2013) Cellular and molecular biology of neuronal Dystonin. *Int Rev*
697 *Cell Mol Biol* **300:** 85-120

698 Glise B, Bourbon H, Noselli S (1995) hemipterous encodes a novel drosophila MAP kinase kinase,
699 required for epithelial cell sheet movement. *Cell* **83:** 451-461

700 Goldstein AY, Wang X, Schwarz TL (2008) Axonal transport and the delivery of pre-synaptic
701 components. *Curr Opin Neurobiol* **18:** 495-503

702 Goodin S, Kane MP, Rubin EH (2004) Epothilones: Mechanism of Action and Biologic Activity.
703 *Journal of Clinical Oncology* **22:** 2015-2025

704 Goryunov D, He CZ, Lin CS, Leung CL, Liem RK (2010) Nervous-tissue-specific elimination of
705 microtubule-actin crosslinking factor 1a results in multiple developmental defects in the mouse brain.
706 *Mol Cell Neurosci* **44:** 1-14

707 Gozes I (2011) Microtubules (tau) as an emerging therapeutic target: NAP (davunetide). *Curr Pharm*
708 *Des* **17:** 3413-3417

709 Halfon MS, Gisselbrecht S, Lu J, Estrada B, Keshishian H, Michelson AM (2002) New fluorescent
710 protein reporters for use with the *Drosophila* Gal4 expression system and for vital detection of
711 balancer chromosomes. *Genesis* **34:** 135-138

712 Hernandez F, Avila J (2007) Tauopathies. *Cell Mol Life Sci* **64:** 2219-2233

713 Hirokawa N, Niwa S, Tanaka Y (2010) Molecular motors in neurons: transport mechanisms and roles
714 in brain function, development, and disease. *Neuron* **68:** 610-638

715 Hoover BR, Reed MN, Su J, Penrod RD, Kotilinek LA, Grant MK, Pitstick R, Carlson GA, Lanier LM,
716 Yuan L-L, Ashe KH, Liao D (2010) Tau Mislocalization to Dendritic Spines Mediates Synaptic
717 Dysfunction Independently of Neurodegeneration. *Neuron* **68:** 1067-1081

718 Jaiswal M, Sandoval H, Zhang K, Bayat V, Bellen HJ (2012) Probing mechanisms that underlie
719 human neurodegenerative disease in *Drosophila*. *Annu Rev Genet* **46:** 371-396

720 Ka M, Kim WY (2015) Microtubule-Actin Crosslinking Factor 1 is required for dendritic arborization
721 and axon outgrowth in the developing brain. *Mol Neurobiol*

722 Kolodziej PA, Jan LY, Jan YN (1995) Mutations that affect the length, fasciculation, or ventral
723 orientation of specific sensory axons in the *Drosophila* embryo. *Neuron* **15:** 273-286

724 Kovacs GG (2015) Invited review: Neuropathology of tauopathies: principles and practice.
725 *Neuropathology and Applied Neurobiology* **41:** 3-23

726 Küppers-Munther B, Letzkus J, Lüer K, Technau G, Schmidt H, Prokop A (2004) A new culturing
727 strategy optimises *Drosophila* primary cell cultures for structural and functional analyses. *Dev Biol*
728 **269:** 459-478

Küppers B, Sánchez-Soriano N, Letzkus J, Technau GM, Prokop A (2003) In developing *Drosophila* neurones the production of gamma-amino butyric acid is tightly regulated downstream of glutamate decarboxylase translation and can be influenced by calcium. *J Neurochem* **84:** 939-951

Landgraf M, Sánchez-Soriano N, Technau GM, Urban J, Prokop A (2003) Charting the *Drosophila* neuropile: a strategy for the standardised characterisation of genetically amenable neurites. *Dev Biol* **260:** 207-225

Langen M, Koch M, Yan J, De Geest N, Erfurth M-L, Pfeiffer BD, Schmucker D, Moreau Y, Hassan BA (2013) *Mutual inhibition among postmitotic neurons regulates robustness of brain wiring in Drosophila*, Vol. 2.

Littleton JT, Bellen HJ, Perin MS (1993) Expression of synaptotagmin in *Drosophila* reveals transport and localization of synaptic vesicles to the synapse. *Development* **118:** 1077-1088

Löhr R, Godenschwege T, Buchner E, Prokop A (2002) Compartmentalisation of central neurons in *Drosophila*: a new strategy of mosaic analysis reveals localisation of pre-synaptic sites to specific segments of neurites. *J Neurosci* **22:** 10357-10367

Lotharius J, Falsig J, van Beek J, Payne S, Dringen R, Brundin P, Leist M (2005) Progressive Degeneration of Human Mesencephalic Neuron-Derived Cells Triggered by Dopamine-Dependent Oxidative Stress Is Dependent on the Mixed-Lineage Kinase Pathway. *The Journal of Neuroscience* **25:** 6329-6342

Luo L, Liao YJ, Jan LY, Jan YN (1994) Distinct morphogenetic functions of similar small GTPases: *Drosophila* Drac1 is involved in axonal outgrowth and myoblast fusion. *Genes Dev* **8:** 1787-1802

Ma Q-L, Zuo X, Yang F, Ubeda OJ, Gant DJ, Alaverdyan M, Kiosea NC, Nazari S, Chen PP, Nothias F, Chan P, Teng E, Frautschy SA, Cole GM (2014) Loss of MAP Function Leads to Hippocampal Synapse Loss and Deficits in the Morris Water Maze with Aging. *The Journal of Neuroscience* **34:** 7124-7136

Martín-Blanco E, Gampel A, Ring J, Virdee K, Kirov N, Tolkovsky AM, Martinez-Arias A (1998) puckered encodes a phosphatase that mediates a feedback loop regulating JNK activity during dorsal closure in Drosophila. *Genes & Development* **12:** 557-570

Morris M, Hamto P, Adame A, Devidze N, Masliah E, Mucke L (2013) Age-appropriate cognition and subtle dopamine-independent motor deficits in aged Tau knockout mice. *Neurobiology of aging* **34:** 1523-1529

Niwa S, Takahashi H, Hirokawa N (2013) (beta)-Tubulin mutations that cause severe neuropathies disrupt axonal transport. *EMBO J* **32:** 1352-1364

Pack-Chung E, Kurshan PT, Dickman DK, Schwarz TL (2007) A *Drosophila* kinesin required for synaptic bouton formation and synaptic vesicle transport. *Nat Neurosci* **10:** 980-989

Pooler AM, Noble W, Hanger DP (2014) A role for tau at the synapse in Alzheimer's disease pathogenesis. *Neuropharmacology* **76, Part A:** 1-8

Prokop A (2013) The intricate relationship between microtubules and their associated motor proteins during axon growth and maintenance. *Neur Dev* **8:** 17

Prokop A, Beaven R, Qu Y, Sánchez-Soriano N (2013) Using fly genetics to dissect the cytoskeletal machinery of neurons during axonal growth and maintenance. *J Cell Sci* **126:** 2331-2341

Prokop A, Küppers-Munther B, Sánchez-Soriano N (2012) Using primary neuron cultures of *Drosophila* to analyse neuronal circuit formation and function. In *The making and un-making of neuronal circuits in Drosophila*, Hassan BA (ed), Vol. 69, pp 225-247. New York: Humana Press

Prokop A, Meinertzhagen IA (2006) Development and structure of synaptic contacts in *Drosophila*. *Semin Cell Dev Biol* **17:** 20-30

774 Prokop A, Uhler J, Roote J, Bate MC (1998) The *kakapo* mutation affects terminal arborisation and
775 central dendritic sprouting of *Drosophila* motorneurons. *J Cell Biol* **143:** 1283-1294

776 Quraishe S, Cowan CM, Mudher A (2013) NAP (davunetide) rescues neuronal dysfunction in a
777 *Drosophila* model of tauopathy. *Mol Psychiatry* **18:** 834-842

778 Roote J, Prokop A (2013) How to design a genetic mating scheme: a basic training package for
779 *Drosophila* genetics. *G3 (Bethesda)* **3:** 353-358

780 Sánchez-Soriano N, Gonçalves-Pimentel C, Beaven R, Haessler U, Ofner L, Ballestrem C, Prokop A
781 (2010) *Drosophila* growth cones: a genetically tractable platform for the analysis of axonal growth
782 dynamics. *Dev Neurobiol* **70:** 58-71

783 Sánchez-Soriano N, Travis M, Dajas-Bailador F, Goncalves-Pimentel C, Whitmarsh AJ, Prokop A
784 (2009) Mouse ACF7 and *Drosophila* Short stop modulate filopodia formation and microtubule
785 organisation during neuronal growth. *J Cell Sci* **122:** 2534-2542

786 Sapir T, Frotscher M, Levy T, Mandelkow EM, Reiner O (2012) Tau's role in the developing brain:
787 implications for intellectual disability. *Hum Mol Genet* **21:** 1681-1692

788 Saxena S, Caroni P (2007) Mechanisms of axon degeneration: From development to disease.
789 *Progress in Neurobiology* **83:** 174-191

790 Schwarz TL (2013) Mitochondrial trafficking in neurons. *Cold Spring Harb Perspect Biol* **5:** a011304

791 Sclip A, Tozzi A, Abaza A, Cardinetti D, Colombo I, Calabresi P, Salmona M, Welker E, Borsello T
792 (2014) c-Jun N-terminal kinase has a key role in Alzheimer disease synaptic dysfunction in vivo. *Cell*
793 *Death Dis* **5:** e1019

794 Serrano-Pozo A, Frosch MP, Masliah E, Hyman BT (2011) Neuropathological alterations in Alzheimer
795 disease. *Cold Spring Harb Perspect Med* **1:** a006189

796 Shao CY, Mirra SS, Sait HB, Sacktor TC, Sigurdsson EM (2011) Postsynaptic degeneration as
797 revealed by PSD-95 reduction occurs after advanced Abeta and tau pathology in transgenic mouse
798 models of Alzheimer's disease. *Acta neuropathologica* **122:** 285-292

799 Shemesh OA, Spira ME (2011) Rescue of neurons from undergoing hallmark tau-induced Alzheimer's
800 disease cell pathologies by the antimitotic drug paclitaxel. *Neurobiol Dis* **43:** 163-175

801 Stagi M, Gorlovoy P, Larionov S, Takahashi K, Neumann H (2006) Unloading kinesin transported
802 cargoes from the tubulin track via the inflammatory c-Jun N-terminal kinase pathway. *The FASEB*
803 *Journal* **20:** 2573-2575

804 Subramanian A, Prokop A, Yamamoto M, Sugimura K, Uemura T, Betschinger J, Knoblich JA, Volk T
805 (2003) Shortstop Recruits EB1/APC1 and Promotes Microtubule Assembly at the Muscle-Tendon
806 Junction. *Current Biology* **13:** 1086-1095

807 Takei Y, Teng J, Harada A, Hirokawa N (2000) Defects in axonal elongation and neuronal migration in
808 mice with disrupted tau and map1b genes. *J Cell Biol* **150:** 989-1000

809 Valakh V, Frey E, Babetto E, Walker LJ, DiAntonio A (2015a) Cytoskeletal disruption activates the
810 DLK/JNK pathway, which promotes axonal regeneration and mimics a preconditioning injury.
811 *Neurobiology of Disease* **77:** 13-25

812 Valakh V, Frey E, Babetto E, Walker LJ, DiAntonio A (2015b) Cytoskeletal disruption activates the
813 DLK/JNK pathway, which promotes axonal regeneration and mimics a preconditioning injury.
814 *Neurobiology of Disease* **77:** 13-25

815 Valakh V, Walker LJ, Skeath JB, DiAntonio A (2013) Loss of the Spectraplakin Short Stop Activates
816 the DLK Injury Response Pathway in Drosophila. *The Journal of Neuroscience* **33:** 17863-17873

Weingarten MD, Lockwood AH, Hwo SY, Kirschner MW (1975) A protein factor essential for microtubule assembly. *Proceedings of the National Academy of Sciences of the United States of America* **72:** 1858-1862

Williams DR (2006) Tauopathies: classification and clinical update on neurodegenerative diseases associated with microtubule-associated protein tau. *Intern Med J* **36:** 652-660

Zhang B, Carroll J, Trojanowski JQ, Yao Y, Iba M, Potuzak JS, Hogan A-ML, Xie SX, Ballatore C, Smith AB, Lee VM-Y, Brunden KR (2012) The Microtubule-Stabilizing Agent, Epothilone D, Reduces Axonal Dysfunction, Neurotoxicity, Cognitive Deficits, and Alzheimer-Like Pathology in an Interventional Study with Aged Tau Transgenic Mice. *The Journal of Neuroscience* **32:** 3601-3611

Zhukareva V, Vogelsberg-Ragaglia V, Van Deerlin VMD, Bruce J, Shuck T, Grossman M, Clark CM, Arnold SE, Masliah E, Galasko D, Trojanowski JQ, Lee VMY (2001) Loss of brain tau defines novel sporadic and familial tauopathies with frontotemporal dementia. *Annals of Neurology* **49:** 165-175

Zschätzsch M, Langen, M., De Geest, N., Williamson, W. R., Lemon, W. C., Oliva, C., Soldano, A., Munck, S., Hiesinger, P. R., Sanchez-Soriano, N., and A. Hassan, B (2014) Regulation of axonal branch refinement by asymmetric EGF-receptor signalling. *eLife 3. doi:10.7554/eLife.01699*

## Figures

**Figure 1.** Tau and Shot are required for the formation of synaptic specialisations in axons. **A)** Primary neurons at 2 DIV obtained from embryos that were wildtype (wt), *tau*$^{-/-}$ , and *tau*$^{-/-}$ with *elav-Gal4* driven expression of *UAS-tau-GFP*; neurons were stained for tubulin (Tub, red) and Syt (light blue). **B)** Quantification of the experiment shown in A, shown as the number of Syt puncta per neuron, normalised to wildtype (the assessed numbers of neurons are indicated in each bar, *** $P_{MW}$<0.001, ** $P_{MW}$<0.01). **C)** Primary *Drosophila* neurons at 2DIV, obtained from embryos that were wildtype (wt), *tau*$^{MR22}$ (*tau*$^{-/-}$), *shot*$^{3}$ (*shot*$^{-/-}$), and *shot*$^{3}$ *tau*$^{MR22}$ (*shot*$^{-/-}$ *tau*$^{-/-}$), co-stained with antibodies against HRP (magenta) and the synaptic proteins (green) Synaptotagmin (Syt) andBruchpilot (Brp); areas emboxed with dashed lines are displayed as magnified insets showing the synaptic staining only. **D)** Quantification of the experiments in C, displayed as number (n.) of Syt and Brp puncta per neuron, normalised to wildtype (the assessed numbers of neurons are indicated in each bar, ***, $P_{MW}$<0.001; **, $P_{MW}$<0.01; *, $P_{MW}$<0.05,). Scale bar: 10µm. A statistics summary of the data shown here is available in Figure 1—source data 1.

**Figure 2.** Tau and Shot regulate the localisation of presynaptic proteins at the embryonic NMJ *in vivo*. **A)** Image show the dorsal segment of inter-segmental motornerves (Landgraf et al, 2003) in stage 16 embryos that were wildtype (wt), $tau^{MR22}$ ($tau^{-/-}$), $shot^{3}$ ($shot^{-/-}$), and $shot^{3}$ $tau^{MR22}$ ($shot^{-/-}$ $tau^{-/-}$), stained with antibodies against Synaptotagmin (Syt, green) and the motorneuron-specific cell membrane protein Fasciclin II (FasII, magenta). Arrowheads depict the distal end of the motoraxons where the nascent NMJs are forming; boxed areas are displayed as enlarged insets showing anti-Syt staining only. Note that cell bodies of sensory neurons contain visible levels of Syt in the mutant (white arrows) but not wildtype neurons (open arrow). **B)** Quantification of the experiments in A, shown as the average intensity of Syt at the nerve ending normalised to wildtype (the sample number or NMJs is indicated in each bar, ***, $P_{MW}<0.001$; **, $P_{MW}<0.01$; *, $P_{MW}<0.05$; ns, not significant $P_{MW}>0.05$). Scale bars: 10 µm. A statistics summary of the data shown here is available in Figure 2—source data 1.

**Figure 3.** Tau and Shot are required for the maintenance of synaptic markers in cultured neurons and the ageing adult fly brain. **A)** Primary neurons at 3 DIV and 26 DIV cultured from embryos that were wildtype or jointly expressing *UAS-*$tau^{RNAi}$ and *UAS-*$shot^{RNAi}$ in all neurons driven by the pan-neuronal driver *elav-Gal4* ($tau^{RNAi}$ $shot^{RNAi}$). Neurons are stained with anti-tubulin and anti-Syt; at 26 DIV, $tau^{RNAi}$ $shot^{RNAi}$ neurons display a reduction in the number of Syt puncta when compared to wildtype. **B)** Quantification of the experiments in A, shown as the number of Syt puncta per neuron at 3 DIV, 18 DIV and 26 DIV, normalised to wildtype controls (the number of assessed neurons is indicated in each bar; ***, $P_{MW}<0.001$; ns, not significant $P_{MW}>0.05$). **C)** A region of *Drosophila* adult brains including the medulla (delimited by dashed lines) where Syt-GFP is expressed in dorsal cluster neurons using *atonal*-Gal4, in the absence (control) or together with $tau^{RNAi}$ and $shot^{RNAi}$ ($tau^{RNAi}$ $shot^{RNAi}$). Brains are stained with anti-GFP at 2-5 days (young) and 24-29 days (old) after eclosion. Note, that GFP-labelled synapses (arrowheads) are decreased in old brains upon *shot* and

*tau* knock-down. **D)** Quantification of the experiments in C, showing the normalised number of Syt-GFP-labelled puncta in old specimen per mean number of puncta in young specimens for the following phenotypes: *ato-Gal4 UAS-syt-GFP* alone (*control*), co-expressing *UAS-tauRNAi* (*tau*$^{RNAi}$), *UAS-shot*$^{RNAi}$ (*shot*$^{RNAi}$), or both knock-down constructs ( *tau*$^{RNAi}$ *shot*$^{RNAi}$; the number of analysed brains is indicated in each bar, *** $P_{MW}$<0.001; ns, not significant $P_{MW}$>0.05). **E)** Brain regions as in C, of animals expressing the membrane marker myr-tdTomato driven by *ato-Gal4* revealing the morphology of the projections of dorsal cluster neurons within the medulla (delimited by dashed lines); brains were from adults at 2-5 days (young) and 24-29 days (old) after eclosure, expressing myr-tdTomato either alone (control) or together with *tau*$^{RNAi}$ and *shot*$^{RNAi}$ (*tau*$^{RNAi}$ *shot*$^{RNAi}$). **F)** Quantification of the experiments in E, displayed as number of branches per axon projecting into the medulla (the number of axons analysed is indicated in each bar; ns, not significant $P_{MW}$>0.05). Scale bar: 10 µm in A and 40 µm in C and E. A statistics summary of the data shown here is available in Figure 3—source data 1.

**Figure 4.** Intracellular transport of synaptic proteins is defective in *shot-tau* mutant neurons. **A**) Primary *Drosophila* neurons at 8HIV, obtained from embryos that were wildtype (wt) and *shot-tau* (*shot*$^{-/-}$ *tau*$^{-/-}$) stained with antibodies against pan-neuronal HRP (magenta in A), Syt (green in A) or nSyb (green in A); nSyb and Syt are reduced in the growth cones (open versus white arrow heads) but enriched in cell bodies (open versus white arrows) of *shot-tau* mutant neurons. **B**) Quantification of the experiments from A, given as the number of nSyb or Syt puncta in axons and growth cones; the number of analysed neurons is given in the bars (***, $P_{MW}$<0.001). **C**) Quantification of various transport parameters generated from live movies of axons of wildtype or *shot-tau* mutant neurons (*shot*$^{-/-}$ *tau*$^{-/-}$) at 8 HIV with *elav-Gal4* driven expression of *UAS-Syt-GFP*. Axonal anterograde and retrograde velocities are subtle or no altered in the axons of *shot-tau* neurons. On the contrary, the numbers of vesicles in axons of *shot-tau* neurons are sharply decreased and increased in the somata (**,

$P_{MW}$<0.01; *, $P_{MW}$<0.05; ns, not significant $P_{MW}$>0.05). **D**) Magnified views of the somata from primary *Drosophila* neurons at 2 DIV, obtained from wildtype (wt) and *shot-tau* mutant embryos (*shot*$^{-/-}$ *tau*$^{-/-}$), co-stained with antibodies against Syt ; To document the protein content within cell bodies, several z stacks per neuron were obtain and project as maximal projection; the cell bodies show higher levels of Syt in *shot-tau* mutant neurons as compared to wildtype (number of assessed cells is indicated in the bars, average staining intensity normalised to wildtype;***, $P_{MW}$<0.001). **E**) The dorsal peripheral nervous system (PNS) of wildtype and*shot-tau* embryos at late stage 16 (stages according to )(Campos-Ortega & Hartenstein, 1997) stained for Syt (green), FasII (red) andthe pan-neuronal nuclear marker Elav (blue). The nascent NMJ at the tip of the inter-segmental motornerve (red) in wildtype contains high levels of Syt (arrowheads) whereas the somata of sensory neurons (blue and grey in insets) contain low levels (open arrows); in *shot-tau* homozygous embryos the somata of sensory neurons have high levels of Syt (arrows and inset), whereas there is only little staining at the nerve tip (open arrowhead). Scale bars: 10 µm in A, 5 µm in D and 5 µm in E. A statistics summary of the data shown here is available in Figure 4—source data 1.

**Figure 5.** Defects in kinesin-3 function mediate synaptic deficits in *shot-tau* mutant neurons. Shot and Tau interacts with Unc-104 and regulate its subcellular distribution. **A**) Primary *Drosophila* neurons at 2 DIV, obtained from embryos which were wildtype, homozygous for *unc104*$^{imac170}$ (*unc104*$^{-/-}$), or triple-heterozygous for *shot*$^{3}$ *tau*$^{MR22}$ *unc104*$^{imac170}$ mutant (shot$^{+/-}$ tau$^{+/-}$ *unc104*$^{+/-}$), co-stained with antibodies against tubulin (Tub, magenta) and Syt (green). The graph shows the quantification of the data including also *unc104*$^{-/+}$ and shot$^{-/-}$ *tau*$^{-/-}$ controls . **B**) Quantification of Synaptotagmin puncta in 2 day old neurons, obtained from embryos that were wildtype or shot$^{-/-}$ *tau*$^{-/-}$ with *elav-Gal4* driven expression of *UAS-unc-104* (compare Figure 1D). **C**) The dorsal peripheral nervous system (PNS) and the central nervous system (CNS) of wildtype and *shot*$^{3}$ *tau*$^{MR22}$ *unc104*$^{imac170}$ triple heterozygous

embryos at late stage 16 (stages according to )(Campos-Ortega & Hartenstein, 1997) stained for Syt (green), FasII (red in upper panel) and the pan-neuronal nuclear marker Elav (blue); for illustration of the imaged tissue see Figure S2A. The nascent NMJ at the tip of the inter-segmental motornerve (red in upper panels) in wildtype contains high levels of Syt (arrowheads) whereas the somata of sensory neurons (blue; demarcated by dashed lines) contain low levels (open arrows); in *shot*$^{3}$ *tau*$^{MR22}$ *unc104*$^{imac170}$ triple heterozygous embryos the somata of sensory neurons have high levels of Syt (arrows), whereas there is only little staining at the nerve tip (open arrowhead). In the ventral nerve cord of wildtype (lower panels), Syt is confined to the neuropile (synapse containing CNS compartment; arrow heads) and excluded from the cortex (compartment with the cell bodies of inter-and motorneurons; empty arrows); in the ventral nerve cord of *shot*$^{3}$ *tau*$^{MR22}$ *unc104*$^{imac170}$ triple heterozygous embryos, there are segmental groups of cell bodies displaying higher Syt levels (arrows). **D**) Primary *Drosophila* neurons at 2 DIV, obtained from wildtype (wt) and *tau-shot* mutant embryos, stained with antibodies against pan-neuronal HRP (magenta) and Unc-104 (green); Unc-104 in distal axon segments (emboxed and magnified in insets) is enriched in wildtype but much weaker in *shot-tau* mutant neurons (chevrons indicate neuronal somata). Data were quantified as average intensity of Unc-104 at the distal end of the axon divided by the average intensity at the soma. **E**) Upper and lower panels show the same locations of late stage 16 embryos as shown in C, but taken from wildtype and *shot-tau* mutant embryos, stained for FasII (magenta) and Unc-104 (green). Note the stark decrease of Unc-104 at the end of motor nerves (open versus white arrow heads) and the unusual accumulations of Unc-104 in the cell bodies of sensory neurons as well as in the CNS cortex in *shot-tau* embryos (open versus white arrows). In all graphs, the number of assessed neurons is indicated in each bar; ***, $P_{MW}<0.001$; *, $P_{MW}<0.05$; ns, not significant $P_{MW}>0.05$; scale bars: 18 µm in A, 5 µm in C/PNS and 35 µm C/CNS, 15 µm in D and E/PNS, 35 µm in E/CNS. A statistics summary of the data shown here is available in Figure 5—source data 1.

**Figure 6.** Microtubule instability mediates aberrant JNK signalling and synaptic defects. **A)** Live imaging of *Drosophila* neurons at 2 DIV, obtained from embryos carrying $tau^{304}$ (a protein trap line where the endogenous tau gene is genomically tagged with GFP) and the microtubule binding protein Jupiter-Cherry. Endogenous Tau (in magenta) is observed in a pattern reminiscent of microtubules, and colocalises with Jupiter (shown in green ) . **B)** Axons of *Drosophila* neurons at 6 HIV with the following genotypes: wildtype (*wt*), $shot^{3}$ ($shot^{-/-}$), $tau^{MR22}$ ($tau^{-/-}$), *tau* rescue ($tau^{-/-}$ *UAS-tau*) and *shot-tau* ($shot^{-/-}$ $tau^{-/-}$). Neurons were treated for 2.5 hrs with vehicle (DMSO) or 20µM nocodazole, fixed and stained with anti-tubulin (Tub, magenta and white) and phalloidin (Pha, green). Only $shot^{3}$, $tau^{MR22}$, and *shot-tau* displayed gaps in their axonal microtubule bundles upon nocodazole treatment, but not wildtype and *tau* mutant embryos with Tau rescue. **C)** Quantification of the experiments in B, indicated as the number of breaks in the microtubule staining per axon (number of analysed neurons is indicated in bars; ***, $P_{MW}<0.001$; **, $P_{MW}<0.01$; ns, not significant $P_{MW}>0.05$). **D)** Embryonic motoraxons of wildtype and *shot-tau* embryos at late stage 16 treated with vehicle (DMSO) or 50 nM of the microtubule stabilising drug epothilone B for 3 hrs and stained with FasII (magenta) and Syt (green); in wildtype, the nascent NMJ at the nerve tip contains high levels of Syt (arrowheads); in *shot-tau* embryos there is only little Syt staining at the nerve tip (open arrowhead). Treatment of *shot-tau* embryos with 50nM epothilenon B increases the levels of Syt at the tip of motornerves (arrowheads). **E)** Quantification of the experiments shown in E, measured as the average intensity of Syt at nascent NMJs and normalised to wildtype (number or assessed NMJ is indicated in bars; ***, $P_{MW}<0.001$; ns, not significant $P_{MW}>0.05$). **F)** Upper (PNS) and lower (CNS) panels show the same locations of late stage 16 wildtype embryos as shown in Fig. 5C, stained for FasII (magenta) and activated phospho-JNK (JNK-P); treatment with 100 µm nocodazole for 2 hrs induced a relocation of JNK-P from nascent NMJs (open versus white arrow heads) to cell bodies of sensory neurons and in the CNS cortex (white versus open arrows). Scale bar: 5

µm in A, 4 µm in B, 10 µm in E, 15 µm in D/PNS and 35 µm in D/CNS. A statistics summary of the data shown here is available in Figure 6—source data 1.

**Figure 7.** Activated JNK correlates with the subcellular localisation of Unc-104 and Syt. Upper (PNS) and lower (CNS) panels in A-C show the same locations of late stage 16 embryos as shown in Fig. 5E, but embryos are of different genotypes and stained with different antibodies, as indicated; genotypes: wildtype (*wt*), *shot*$^{3}$ (*shot*$^{-/-}$), *tau*$^{MR22}$ (*tau*$^{-/-}$), *shot-tau* (*shot*$^{-/-}$ *tau*$^{-/-}$), *elav-Gal4* driven expression of *UAS-hep*$^{ac}$ (*UAS-hep*$^{ac}$); used antibodies detect FasII (magenta), Syt (green), Unc-104 (green), activated phospho-JNK (JNK-P). **A)** In wildtype, JNK-P is high at nerve endings (white arrow heads) and below detection levels in cell bodies of sensory neurons and in the CNS cortex (open arrows); this pattern is inverted in *tau*$^{MR22}$ and *shot*$^{3}$ mutant embryos and even stronger in *shot-tau* embryos, i.e. Syt is reduced at nerve endings (open arrow heads) and upregulated in cell bodies (white arrows). **B, C)** Artificial activation of JNK with neuronal expression of Hep$^{ac}$ suppresses high levels of Unc-104 and Syt at nascent NMJs (open versus white arrow heads) and increases their levels in cell bodies (white versus open arrows). Scale bars: 15 µm in PNS panels and 35 µm in CNS panels.

**Figure 8.** Inhibition of the JNK pathway rescues synaptic defects in *shot-tau* mutant neurons. **A**) primary *Drosophila* neurons at 2 DIV, obtained from embryos of the following genotypes: wildtype (wt), *elav-Gal4* driven expression of *UAS-hep*$^{ac}$ (*UAS-hep*$^{ac}$), *tau*$^{MR22}$ (*tau*$^{-/-}$), *wnd*$^{2}$ (*wnd*$^{-/-}$), *tau*$^{-/-}$ with *elav-Gal4* driven expression of *UAS*-puc, *tau*$^{MR22}$ *kay*$^{2}$ (*tau*$^{-/-}$ *kay*$^{-/-}$) and *shot*$^{3}$ *tau*$^{MR22}$ *wnd*$^{2}$ (*shot*$^{-/-}$ *tau*$^{-/-}$ *wnd*$^{-/-}$), all stained with antibodies against tubulin (tub, magenta) and Syt (green). Insets correspond to emboxed areas and show a magnified view of the Syt staining. **B**) Quantification of experiments in A, shown as the number of Syt puncta normalised to wildtype (number of assessed neurons is shown in the bars, ***, $P_{MW}$<0.001; **, $P_{MW}$<0.01; *, $P_{MW}$<0.05; ns, not significant $P_{MW}$>0.05). **C)** Inter-segmental motornerves in the dorsal area of wildtype and *shot*$^{3}$ mutant embryos at late stage 16,

stained against FasII (magenta) and Syt (green); insets correspond to emboxed areas and show a magnified view of the most dorsal nascent NMJs stained for Syt; note the rescue of Syt localisation if Wnd is absent in *tau-shot* mutant background. **D)** Quantification of the experiments in C, measured as the average intensity of Syt normalised to wt (number of assessed NMJs is shown in the bars; ***, $P_{MW}$<0.001; *, $P_{MW}$<0.01). **E)** A region of *Drosophila* adult brains including the medulla; UAS-nSyb-GFP is expressed in dorsal cluster neurons using *atonal*-Gal4, either alone (control), together with $tau^{RNAi}$ and $shot^{RNAi}$ ($tau^{RNAi}$ $shot^{RNAi}$) or together with $tau^{RNAi}$, $shot^{RNAi}$ *and* UAS-$bsk^{DN}$. Brains are shown at 2-6 days (young) and 26-30 days after eclosion (old); GFP-labelled synapses are decreased in old brains with *shot-tau* knock-down when compared to controls, and this effect is rescued by the expression of $Bsk^{DN}$. **F)** Quantification of experiments in E, shown as number of GFP-labelled synapses in old specimen per mean number of GFP-labelled synapses in young specimens of the respective genotype (number of analysed brains is indicated in the bars; ***, $P_{MW}$<0.001; **, $P_{MW}$<0.01). Scale bars: 5 µm in A, 10 µm in C and 40 µm in E. A statistics summary of the data shown here is available in Figure 8—source data 1.

**Figure 9.** Schematic model of proposed function for Tau and Shot .

A) Neurons illustrating different phenotypes: in wildtype neurons (wt), microtubules are stable (green line) and levels of Unc-104 (red square), synaptic markers (yellow dots) and p-JNK (turquoise background) are high in axon tips; in shot-tau mutant neurons, microtubules are unstable (stippled green lines), and the above listed proteins accumulate in cell bodies (soma); ubiquitous activation of JNK (↑JNK) causes similar somatic accumulation of Unc-104 and synaptic markers; down-regulation of JNK (↓JNK) rescues the *shot-tau* mutant phenotypes. B,C) Schematic representation of the underlying mechanisms: In wildtype neurons (A), Unc-104 is activated (Unc*) and mediates axonal transport of synaptic proteins (yellow arrow) to the axon tip, where we propose (?) that active JNK inhibits Unc-104, thus releasing its cargo for synaptic incorporation. In *shot-tau* mutant neurons, unstable

microtubules cause upregulation of JNK in the soma, thus inhibiting Unc-104 and trapping it as well as its cargo proteins in the soma.

**Supplementary figures**

**Figure 1 - figure supplement 1.** Co-localisation of presynaptic markers reveals presynaptic specialisations. Primary *Drosophila* neurons at 2 DIV co-stained with antibodies against the neuronal marker HRP (red) and different presynaptic proteins (green) including Synaptotagmin (Syt), Synapsin (Syn), neuronal Synaptobrevin (nSyb) or Bruchpilot (Brp); whole neurons are shown, with chevrons indicating somata and the emboxed areas indicating the distal axons shown as threefold manified close-ups; presynaptic proteins show a high degree of co-localisation in the axons, 91% co-localisation of Synapsin (Syn) and Synaptotagmin (Syt) labelled spots (sample size= 24 neurons), 84.7% of Syt and Bruchpilot (Brp) (sample size= 8 neurons), and 81% of neuronal Synaptobrevin (nSyb) with Brp (sample size= 8 neurons), suggesting that the majority of dots represent presynaptic specialisations. Scale bar: 10µm

**Figure 1 - figure supplement 2.** Rescues experiments with Shot and Tau demonstrate redundant roles in synapses. **A)** Primary neurons at 2 DIV obtained from embryos that were wildtype (wt), *shot*$^{-/-}$ with *elav-Gal4* driven expression of *UAS-shot-GFP, shot*$^{-/-}$ with *sca-Gal4* driven expression of *UAS-tau-GFP*, and *tau*$^{-/-}$ with *elav-Gal4* driven expression of *UAS-shot-GFP*; neurons were stained for tubulin (Tub, magenta) and Syt (green). **B)** Quantification of the experiment in A, shown as the number of Syt puncta per neuron, normalised to wildtype (the assessed numbers of neurons are indicated in each bar, *** $P_{MW}<0.001$; *, $P_{MW}<0.05$; ns, not significant $P_{MW}>0.05$). Scale bar: 10µm. A statistics summary of the data shown here is available in Figure 1 - supplement 3 source data 1.

**Figure 2 - figure supplement 1.** Schematic drawings of embryonic tissues analysed in this study. A) Schematic horizontal view of the embryonic nervous system (brain; OL, optic lobe; vNC, ventral nerve cord) showing an exemplary motorneuron (dark blue), muscle (green) and sensory neuron (red). Note that cell bodies in the nervous system lie in the cortex (Cx), i.e. outside the synaptic area (Np, neuropile), and that sensory neurons are positioned in the periphery, often adjacent to synaptic endings of motorneurons (NMJs, neuromuscular junctions). Synapses are shown as yellow dots. The stippled blue frame shows the area (rotated 90 degrees clockwise) shown in Figures 5C, 5D, 8F. B) More detailed representation of the periphery with muscles, motorneuronal projections and sensory neurons (same colours as in A). The stippled blue frame emboxes the area shown in Figures 2, 4E, 5C, 5E, 6D, 6F, 7 and 8C, including an arrow head pointing at the most dorsal NMJ and arrow indicating somata of sensory neurons.

**Figure 3 - figure supplement 1.** Delayed effect of RNAi mediated knock-down of Shot and Tau. **A)** Primary neurons at 3 DIV and 25 DIV cultured from embryos that were wildtype or jointly expressing *UAS-tau*$^{RNAi}$ and *UAS-shot*$^{RNAi}$ in all neurons driven by the pan-neuronal driver *elav-Gal4* (*tau*$^{RNAi}$ *shot*$^{RNAi}$). Neurons are stained with antibodies against Tau, Shot and Tubulin (red, green and blue respectively); images on the right show: a selected axon segment taken from the main image (top) followed by grey scale images of the separated channels for Tau (2$^{nd}$ from top), Shot (3$^{rd}$ from top) and Tubulin (bottom). At 25 DIV, *tau*$^{RNAi}$ *shot*$^{RNAi}$ neurons display a reduction in both Tau and Shot when compared to wildtype. **B)** Quantification of the experiments in A, shown as mean intensity of Tau or Shot signal per neuron at 3 DIV and 25 DIV, normalised to wildtype controls (30-39 neurons were assessed per genotype; ***, $P_{MW}<0.001$; **, $P_{MW}<0.01$; ns, not significant $P_{MW}>0.05$). Comparative data for *shot*$^{3}$ and *tau*$^{MR22}$ homozygous mutant neurons are given as control, indicating low Tau background staining and incomplete knock-down of Tau at 3 DIV, but high Shot background

suggesting strong or complete Shot knock-down at 25 DIV. A statistics summary of the data shown here is available in Figure 3 - supplement 1 source data 1.

**Figure 3 - figure supplement 2.** Schematic drawings of brain areas analysed in this study. Dorso-fronto-lateral view onto a schematic adult CNS composed of the brain and ventral nerve cord (vNC). Beige areas indicate some synaptic areas, in particular the ventral nerve cord neuropile (Np) and the optic lobes (OL) composed of lamina (1), medulla (2), lobula (3) and lobula plate (4). DCN neurons project to the optic lobe of the contralateral brain half where they branch out in a layered fashion. The blue stippled frame and image inset embox the area (rotated 90 degrees counterclockwise) shown in Figures 3E and 8E without and with synaptic markers (yellow dots), respectively.

**Figure 3 - figure supplement 3.** Loss of function mutations in *shot* and *tau* induce morphological changes. **A-D)** Representative examples of the shape of primary neurons at 2 DIV obtained from embryos that were wildtype (wt, A), $shot^{3}\ tau^{MR22}$ ($shot^{-/-}\ tau^{-/-}$ B), $shot^{-/-}\ tau^{-/-}$ with *elav-Gal4* driven expression of *UAS-unc-104* ($shot^{-/-}\ tau^{-/-}$ *UAS-unc-104,* C) and $shot^{3}\ tau^{MR22}\ wnd^{2}$ ($shot^{-/-}\ tau^{-/-}\ wnd^{-/-}$ D). **E-F)** Quantification of morphological parameters of experiment in A-D, including the length of axons (E) and the number of branches (F), (the assessed numbers of neurons are indicated in each bar, *** $P_{MW}<0.001$; ns, not significant $P_{MW}>0.05$). Note that $wnd^{2}$ ($wnd^{-/-}$) restored the number of branches in *shot-tau* mutant neurons, suggesting that JNK not only mediates synapse regulation but also morphogenetic processes downstream of the Shot-Tau deficiency. A statistics summary of the data shown here is available in Figure 3 - supplement 3 source data 1.

**Figure 3 - figure supplement 4.** RNAi-mediated knock-down of Shot and Tau has no effect on axonal length and branch number. **A-B)** Representative examples of the shape of primary neurons at 3, 18 and 26 DIV obtained from embryos that were wildtype (wt, A) or jointly

expressing *UAS-tau$^{RNAi}$* and *UAS-shot$^{RNAi}$* in all neurons driven by the pan-neuronal driver *elav-Gal4* (*tau$^{RNAi}$ shot$^{RNAi}$*, B). **C-D)** Quantification of morphological parameters of experiment in A-B, including the length of axons (C) and the number of branches (D), (the assessed numbers of neurons are indicated in each bar, ns, not significant $P_{MW}$>0.05). A statistics summary of the data shown here is available in Figure 3 - supplement 4 source data 1.

**Figure 5 - figure supplement 1.** Expression of Unc-104 rescues synaptic defects in aged adult brains. **A)** A region of *Drosophila* adult brains including the medulla (see illustration in Figure 3 - figure supplement 2); UAS-nSyb-GFP is expressed in dorsal cluster neurons using *atonal*-Gal4, either alone (control), together with tau$^{RNAi}$ and *shot$^{RNAi}$* (*tau$^{RNAi}$ shot$^{RNAi}$*) or together with tau$^{RNAi}$, *shot$^{RNAi}$ and* UAS-*unc-104* (*tau$^{RNAi}$ shot$^{RNAi}$ UAS-unc-104*). Brains are shown at 2-6 days (young) and 26-30 days after eclosion (old); GFP-labelled synapses are decreased in old brains with *shot-tau* knock-down when compared to controls, and this effect is rescued by the expression of Unc-104. **B)** Quantification of experiments in A, shown as number of GFP-labelled synapses in old specimen per mean number of GFP-labelled synapses in young specimens of the respective genotype (number of analysed brains is indicated in the bars; ***, $P_{MW}$<0.001; **, $P_{MW}$<0.01; ns, not significant $P_{MW}$>0.05). Scale bars: 5 µm in A. A statistics summary of the data shown here is available in Figure 5 - supplement 2 source data 1.

**Figure 6 - figure supplement 1.** Treatment of *shot-tau* mutant neurons with epothilone B, increases the localisation of JNK-P at axonal tips. **A)** Embryonic motoraxons of wildtype and *shot-tau* embryos at late stage 16 treated with vehicle (DMSO) or 50 nM of the microtubule stabilising drug epothilone B for 3 hrs and stained with FasII (magenta) and JNK-P (green); In wildtype, JNK-P is high at nerve endings (white arrow heads) and below detection levels in cell bodies of sensory neurons and in the CNS cortex (open arrows). This pattern is

inverted in *shot-tau* embryos where JNK-P levels are low at nerve tips (open arrowhead) and high in cell bodies of sensory neurons and in the CNS cortex (white arrows). Treatment of *shot-tau* embryos with 50nM epothilone B increases the levels of JNK-P at the tip of motornerves (white arrowheads). **B)** Quantification of the experiments shown in A, measured as the average intensity of JNK-P at nascent NMJs and normalised to wildtype (number of assessed NMJ is indicated in bars; ***, $P_{MW}$<0.001). Scale bars: 15 µm in PNS panels and 35 µm in CNS panels. A statistics summary of the data shown here is available in Figure 6 - supplement 1 source data 1.

**Figure 8 - figure supplement 1.** Attenuation of the JNK pathway rescues aberrant Unc-104 localisation in *shot-tau* mutant neurons in culture. **A**) Primary *Drosophila* neurons at 2 DIV, obtained from wildtype (wt) and *shot*$^{3}$ *tau*$^{MR22}$ *wnd*$^{2}$ mutant embryos (*shot*$^{-/-}$ *tau*$^{-/-}$ *wnd*$^{-/-}$), stained with antibodies against pan-neuronal HRP (magenta) and Unc-104 (green); Unc-104 in distal axon segments (emboxed and magnified in insets) is enriched in wildtype and in *shot*$^{-/-}$ *tau*$^{-/-}$ *wnd*$^{-/-}$ mutant neurons (chevrons indicate neuronal somata). This is in contrast to *shot-tau* mutant neurons, in which Unc-104 in distal axon segments is much weaker (for reference see Figure 5 D). **B**). Data were quantified as average intensity of Unc-104 at the distal end of the axon divided by the average intensity at the soma (**, $P_{MW}$<0.01). Scale bars: 5 µm in A. A statistics summary of the data shown here is available in Figure 8 - supplement 1 source data 1.

**Figure 8 - figure supplement 2.** Attenuation of the JNK pathway rescue aberrant unc-104 localisation in *shot-tau* mutant embryos. **A**) The dorsal peripheral nervous system (PNS) and the central nervous system (CNS) of wildtype wildtype, *shot*$^{3}$ *tau*$^{MR22}$ and *shot*$^{3}$ *tau*$^{MR22}$ *wnd*$^{2}$ mutant embryos (*shot*$^{-/-}$ *tau*$^{-/-}$ *wnd*$^{-/-}$) at late stage 16 stained with stained with FasII (red), Unc-104 (green) and elav (blue) for the PNS panels and FasII (magenta) and Unc-104 (green) in the CNS panels. Note the stark decrease of Unc-104 at the end of motor nerves

(open versus white arrow heads) and the unusual accumulations of Unc-104 in the cell bodies of sensory neurons as well as in the CNS cortex in *shot-tau* embryos (open versus white arrows). This is in contrast to *shot*$^{-/-}$ *tau*$^{-/-}$ *wnd*$^{-/-}$ mutant neurons in which Unc-104 is increased at the end of motor nerves and decreased in the cell bodies of sensory neurons as well as in the CNS cortex. Scale bars: 15 µm in PNS panels and 35 µm in CNS panels.

**Source data**

**Figure 1-source data 1.** Summary of the statistics from Figure 1B and C.

**Figure 1-supplement 2 source data 1.** Summary of the statistics from Figure 1-supplement 2B.

**Figure 2-source data 1.** Summary of the statistics from Figure 2B.

**Figure 3-source data 1.** Summary of the statistics from Figure 3B. D, F.

**Figure 3-supplement 1 source data 1.** Summary of the statistics from Figure 3-supplement 1B

**Figure 3-supplement 3 source data 1.** Summary of the statistics from Figure 3-supplement 3E and F.

**Figure 3-supplement 4 source data 1.** Summary of the statistics from Figure 1-supplement 3C and D

**Figure 4-source data 1.** Summary of the statistics from Figure 4B-D.

**Figure 5-source data 1.** Summary of the statistics from Figure 5.

**Figure 5-supplement 1 source data 1.** Summary of the statistics from Figure 5-supplement1B.

**Figure 6-source data 1.** Summary of the statistics from Figure 6C and E.

**Figure 6-supplement 1 source data 1.** Summary of the statistics from Figure 6-supplement 1B

**Figure 8-source data 1.** Summary of the statistics from figure 8B, D and F.

**Figure 8-supplement 1 source data 1.** Summary statistics from Figure 8-supplement 1B

## Supplementary movies

**Movie S1.** Live imaging of *Drosophila* neurons at 2 DIV, obtained from embryos carrying *tau*$^{304}$ (a protein trap line where the endogenous tau gene is genomically tagged with GFP) and the microtubule binding protein Jupiter-Cherry. Endogenous Tau (in green) is observed in a pattern reminiscent of microtubules, and colocalises with Jupiter (shown in red). The time laps were obtained every 15 seconds with a 3i Marianas Spinning Disk Confocal Microscope.

Fig-1

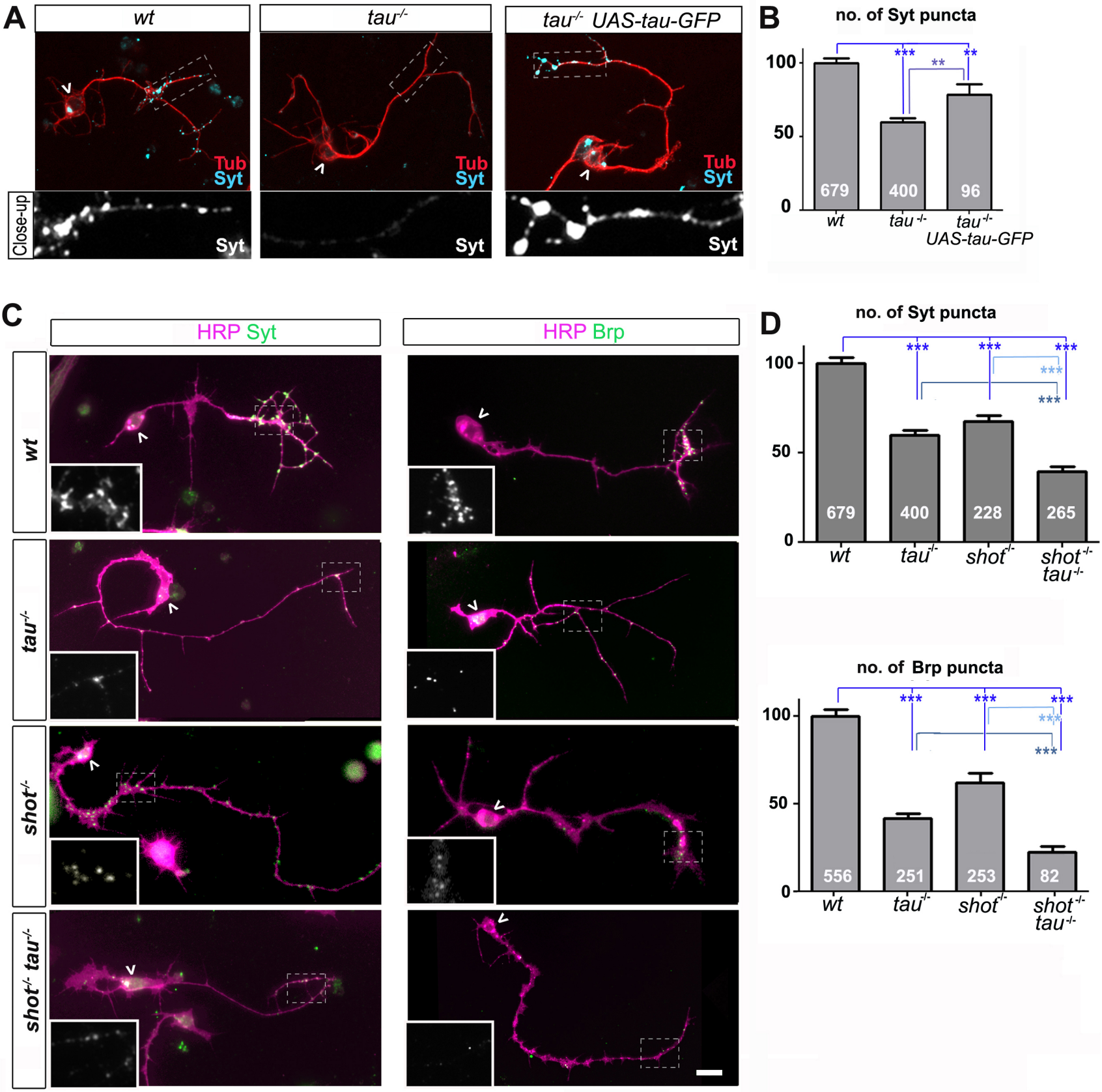
A
wt
tau-/-
tau-/- UAS-tau-GFP
Tub
Syt
Close-up
Syt
B
no. of Syt puncta
100
50
0
679
400
96
wt
tau-/-
tau-/-
UAS-tau-GFP
***
**
**
C
HRP Syt
HRP Brp
wt
tau-/-
shot-/-
shot-/- tau-/-
D
no. of Syt puncta
679
400
228
265
wt
tau-/-
shot-/-
shot-/-
tau-/-
no. of Brp puncta
556
251
253
82

Fig-1S1

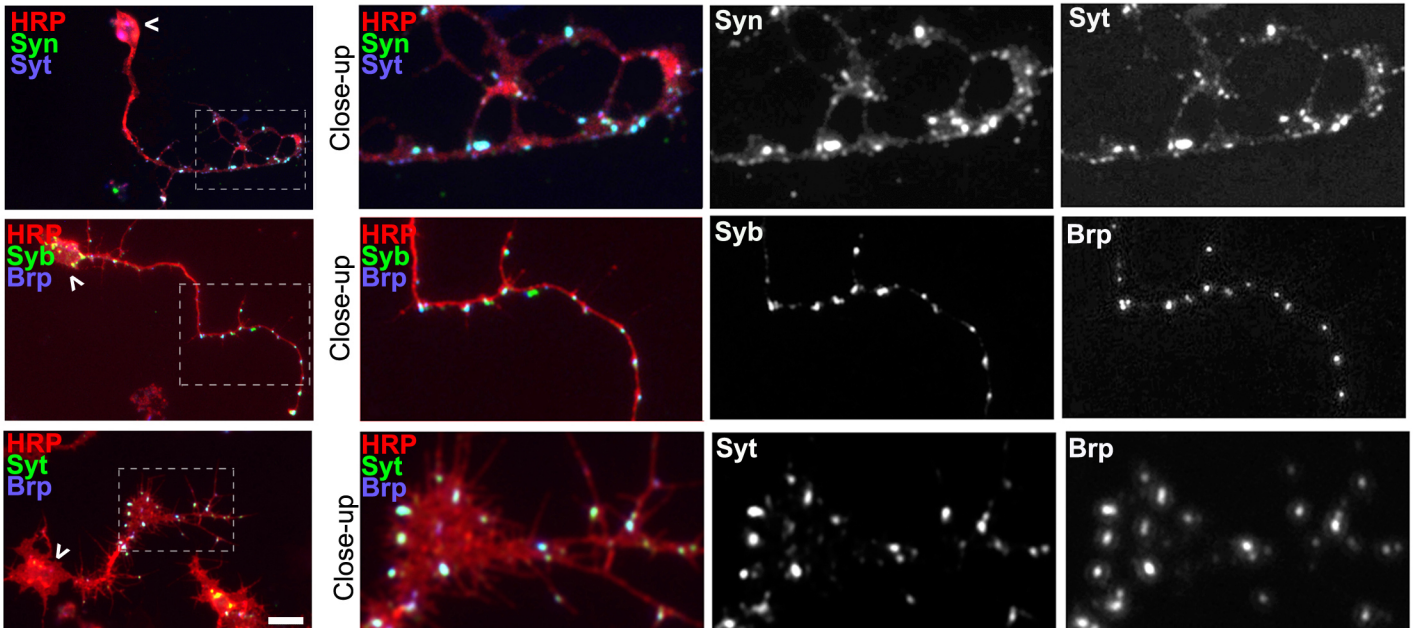
HRP
Syn
Syt
Close-up
HRP
Syn
Syt
Syn
Syt
HRP
Syb
Brp
Close-up
HRP
Syb
Brp
Syb
Brp
HRP
Syt
Brp
Close-up
HRP
Syt
Brp
Syt
Brp

Fig-1S2

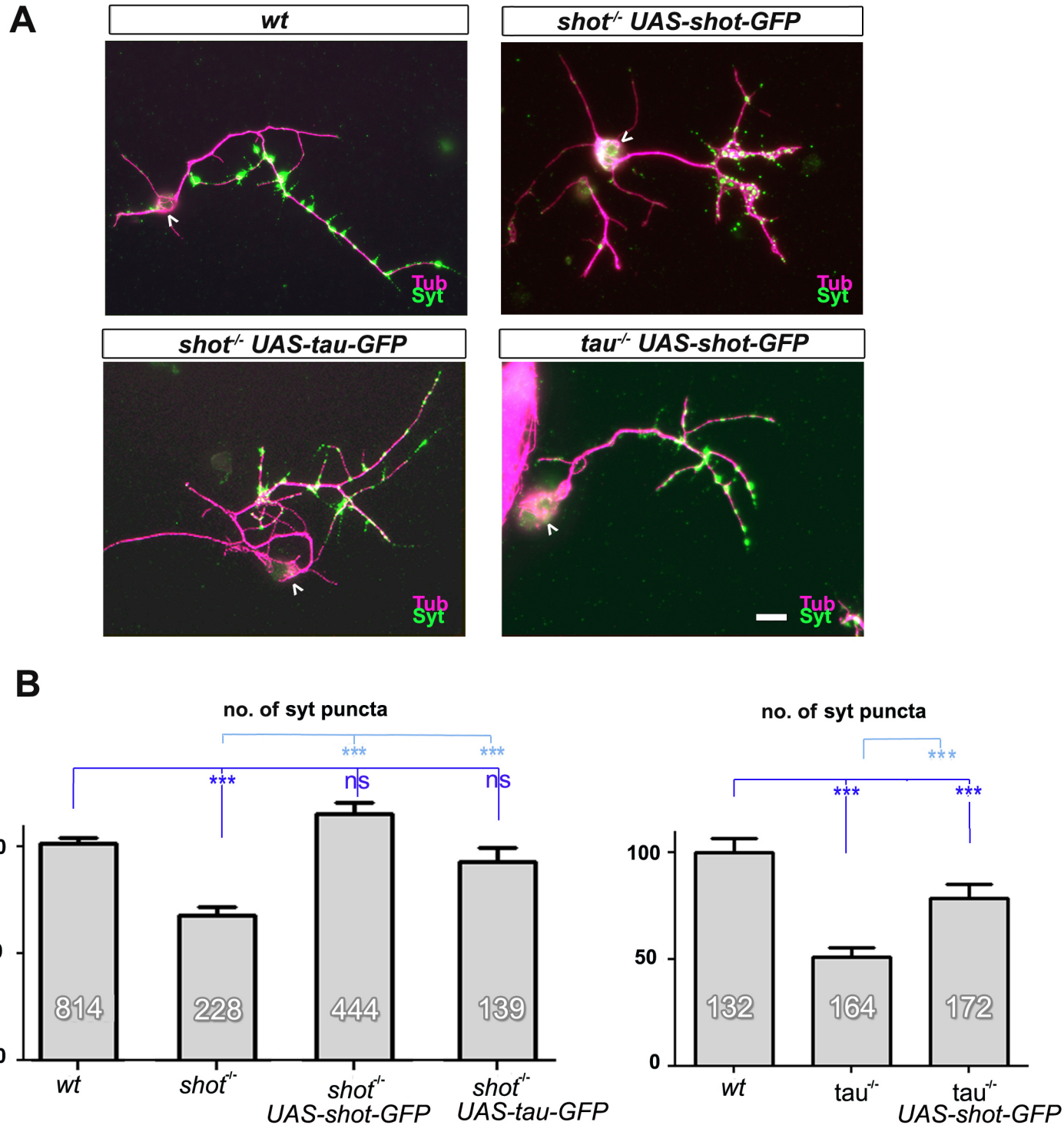
A
wt
shot-/- UAS-shot-GFP
shot-/- UAS-tau-GFP
tau-/- UAS-shot-GFP
Tub
Syt
B
no. of syt puncta
***
***
***
ns
ns
100
50
0
814
228
444
139
wt
shot-/-
shot-/- UAS-shot-GFP
shot-/- UAS-tau-GFP
no. of syt puncta
***
***
***
100
50
0
132
164
172
wt
tau-/-
tau-/- UAS-shot-GFP

Fig-2

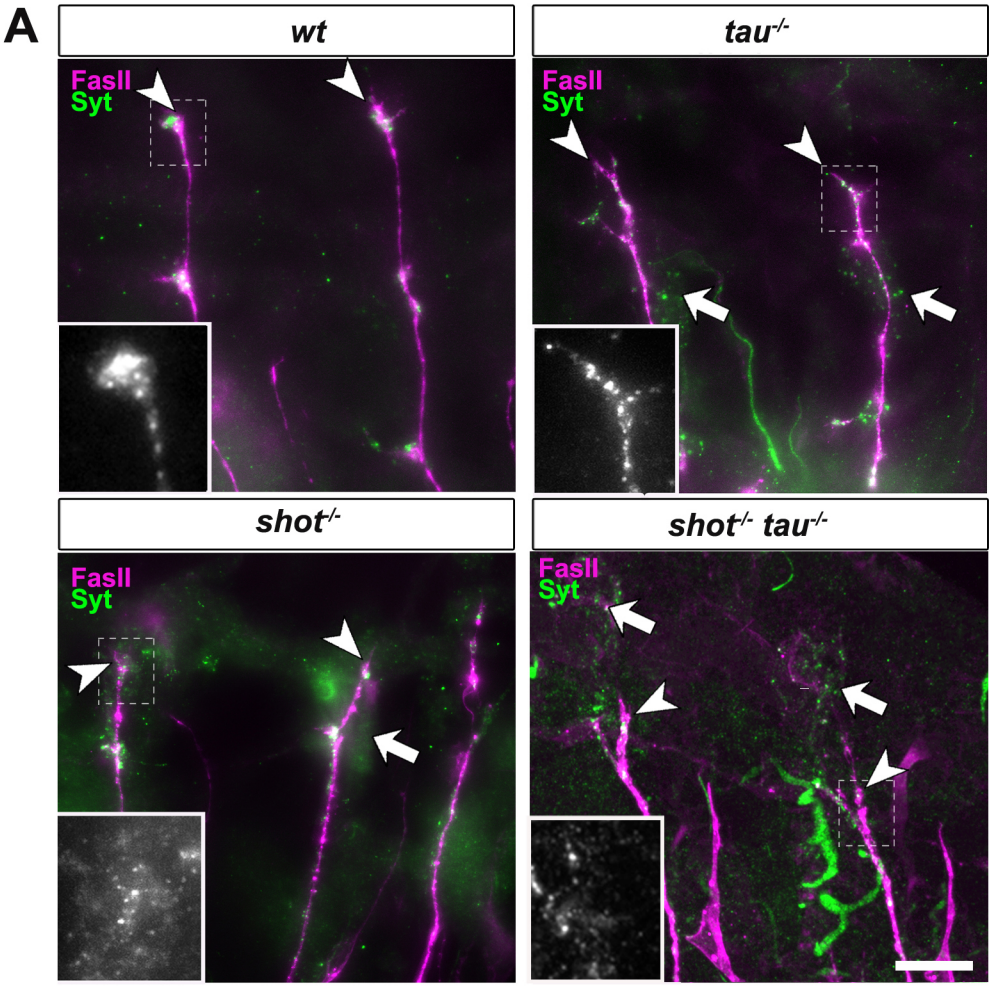
A
wt
tau-/-
shot-/-
shot-/- tau-/-
FasII
Syt

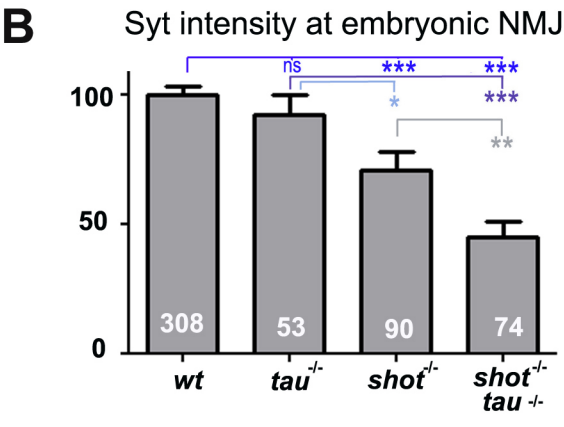
B
Syt intensity at embryonic NMJ
ns
***
***
*
***
**
100
50
0
308
53
90
74
wt
tau-/-
shot-/-
shot-/-
tau -/-

Fig-2S1

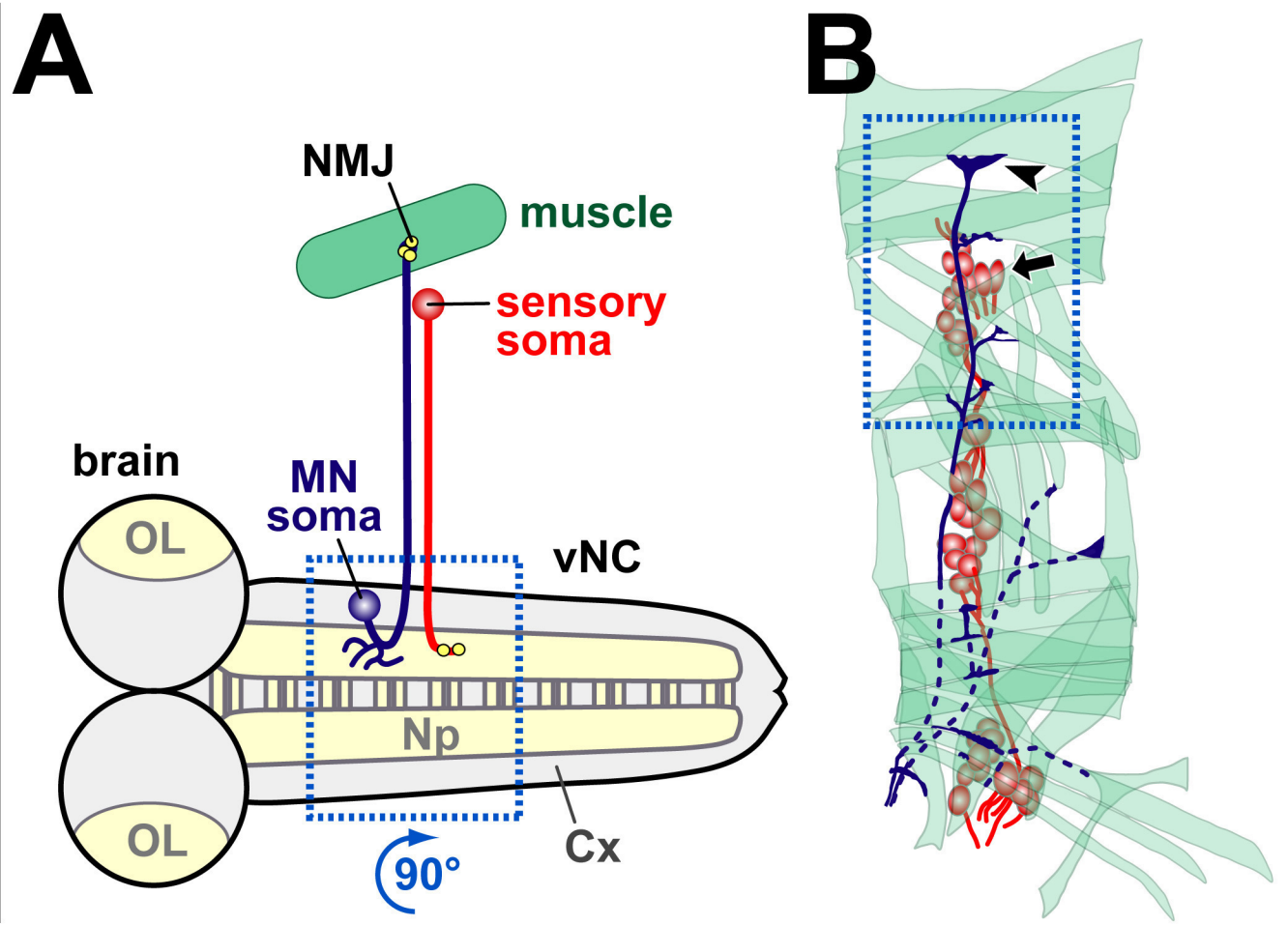

Fig-3

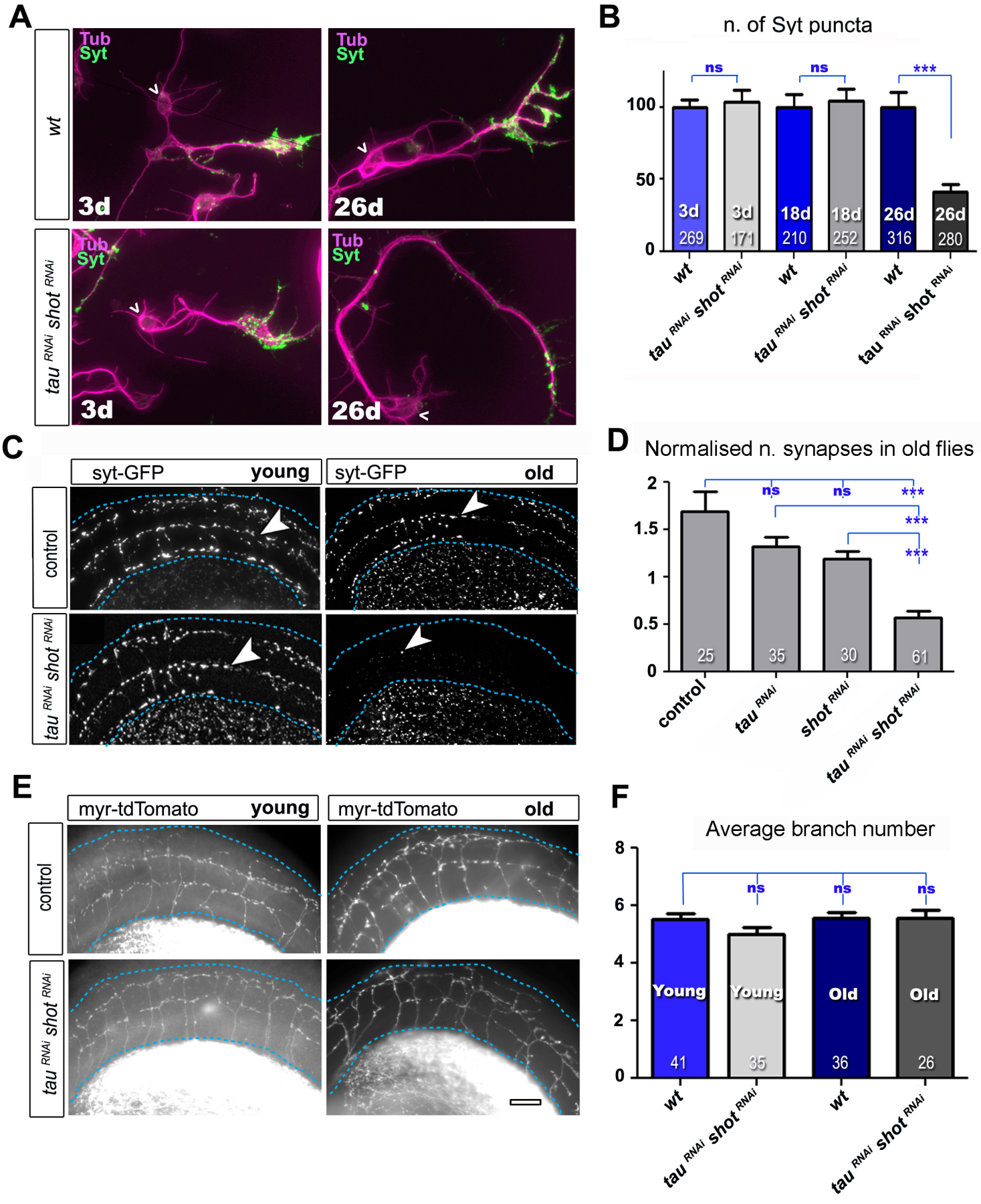
A
wt
tau RNAi shot RNAi
Tub
Syt
3d
26d
B
n. of Syt puncta
ns
ns
***
100
50
0
3d
269
3d
171
18d
210
18d
252
26d
316
26d
280
wt
tau RNAi shot RNAi
C
syt-GFP
young
old
control
tau RNAi shot RNAi
D
Normalised n. synapses in old flies
2
1.5
1
0.5
0
25
35
30
61
control
tau RNAi
shot RNAi
tau RNAi shot RNAi
E
myr-tdTomato
young
old
control
tau RNAi shot RNAi
F
Average branch number
8
6
4
2
0
Young
41
Young
35
Old
36
Old
26
wt
tau RNAi shot RNAi

Fig-3 S1

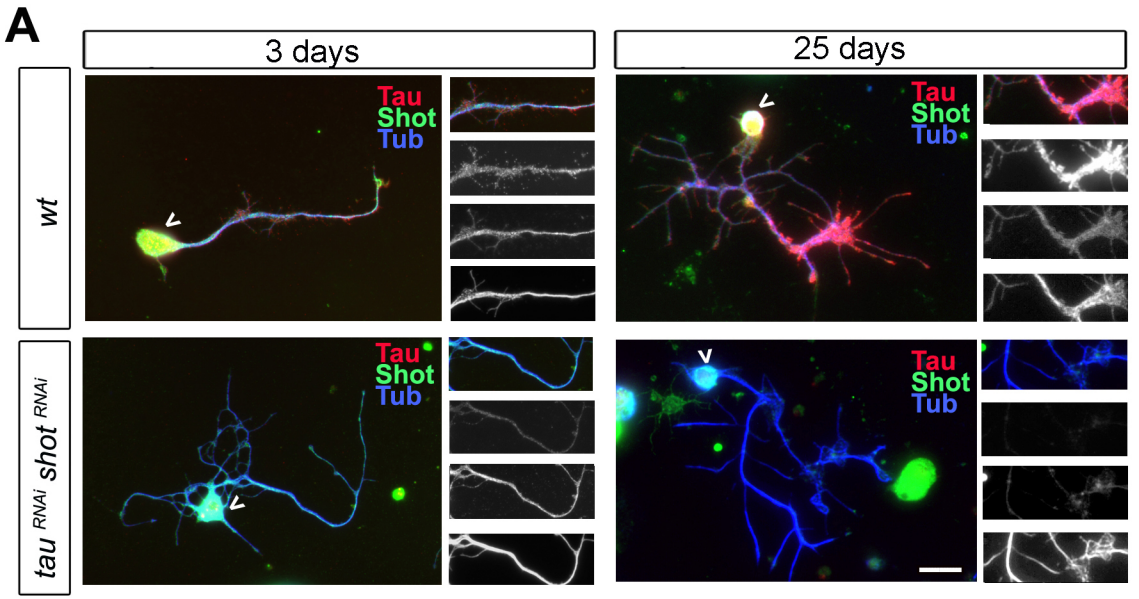
A
3 days
25 days
wt
tau RNAi shot RNAi
Tau
Shot
Tub

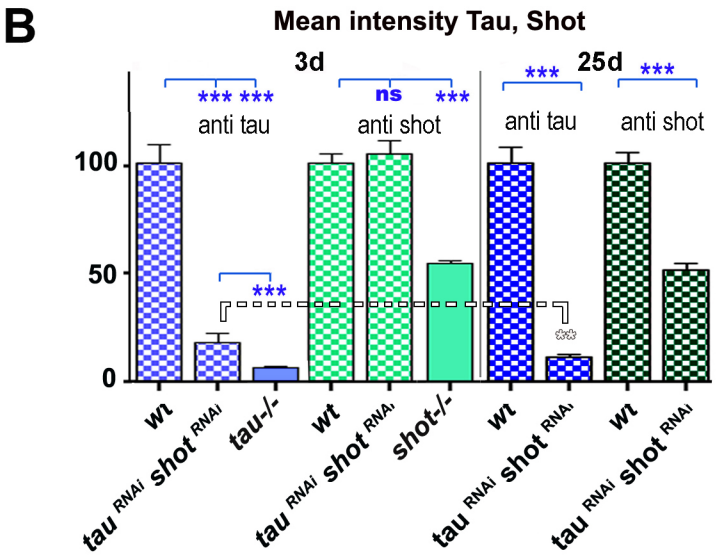
B
Mean intensity Tau, Shot
3d
25d
anti tau
anti shot
anti tau
anti shot
***
ns
100
50
0
wt
tau RNAi shot RNAi
tau-/-
shot-/-

Fig-3S2

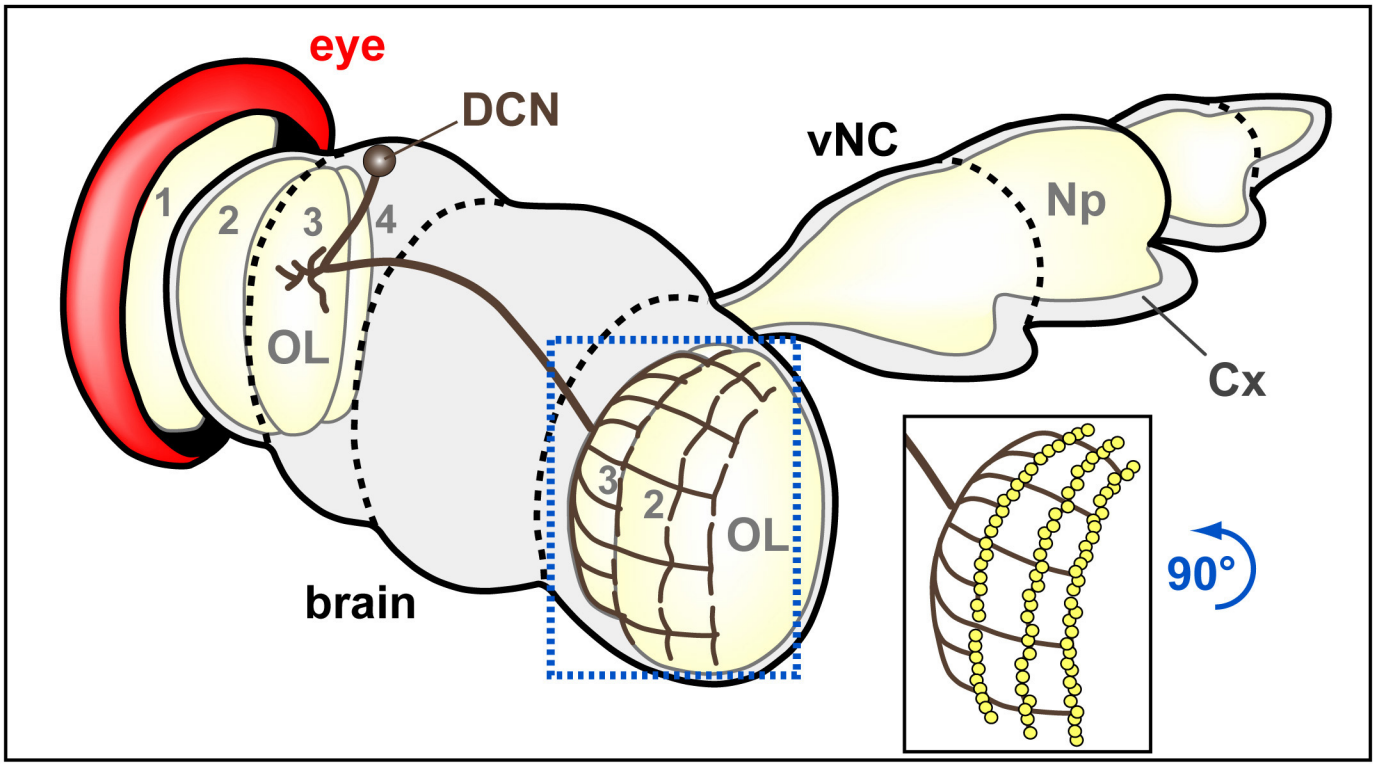

Fig-3S3

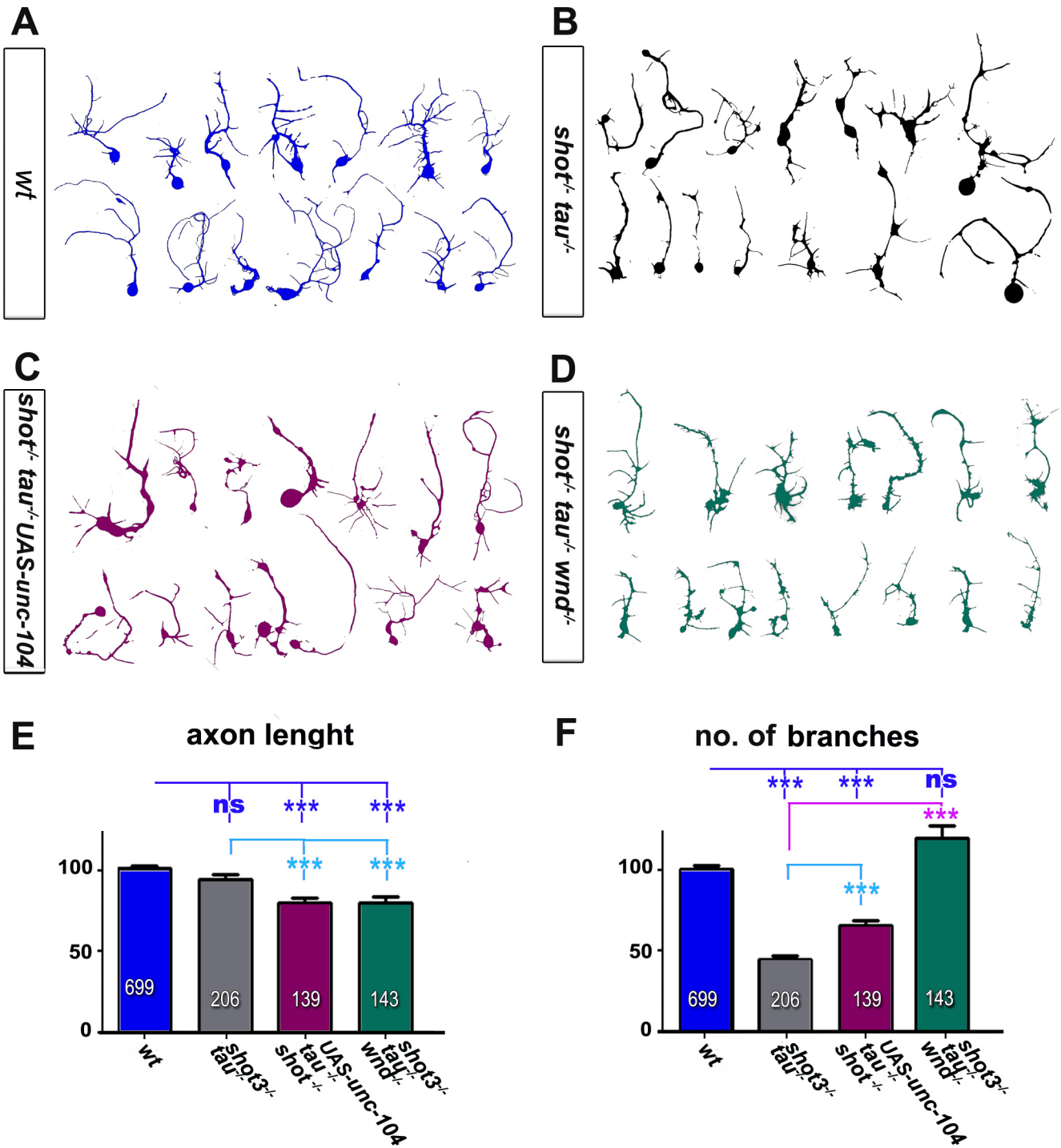
A
wt
B
shot-/- tau-/-
C
shot-/- tau-/- UAS-unc-104
D
shot-/- tau-/- wnd-/-
E
axon lenght
ns
***
***
***
***
100
50
0
699
206
139
143
wt
shot3-/- tau-/-
shot-/- tau-/- UAS-unc-104
shot3-/- tau-/- wnd-/-
F
no. of branches
***
***
ns
***
***
100
50
0
699
206
139
143
wt
shot3-/- tau-/-
shot-/- tau-/- UAS-unc-104
shot3-/- tau-/- wnd-/-

Fig-3S4

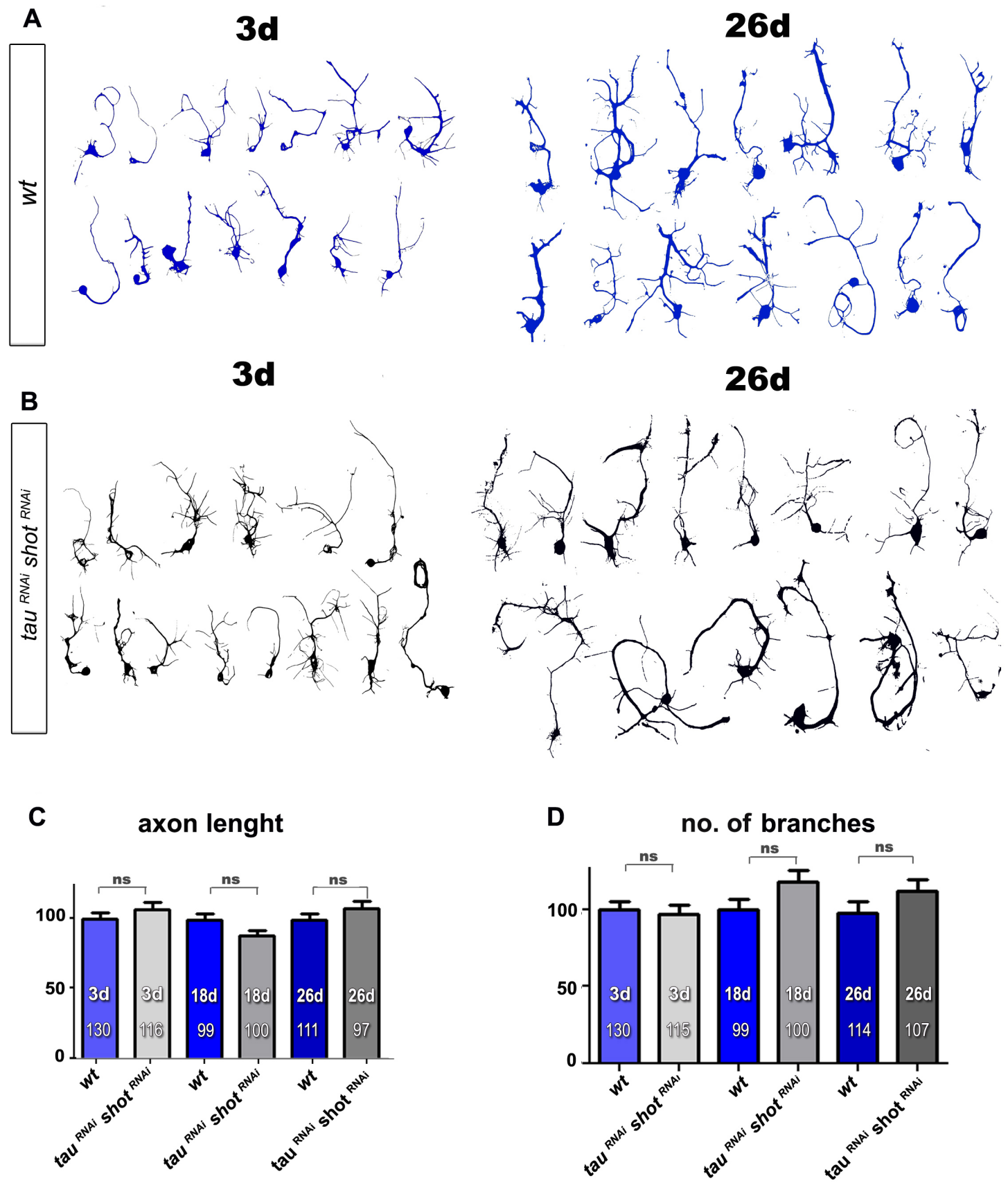
A
3d
26d
wt
B
3d
26d
tau RNAi shot RNAi
C
axon lenght
ns
ns
ns
100
50
0
3d
130
3d
116
18d
99
18d
100
26d
111
26d
97
wt
tau RNAi shot RNAi
wt
tau RNAi shot RNAi
wt
tau RNAi shot RNAi
D
no. of branches
ns
ns
ns
100
50
0
3d
130
3d
115
18d
99
18d
100
26d
114
26d
107
wt
tau RNAi shot RNAi
wt
tau RNAi shot RNAi
wt
tau RNAi shot RNAi

Fig-4

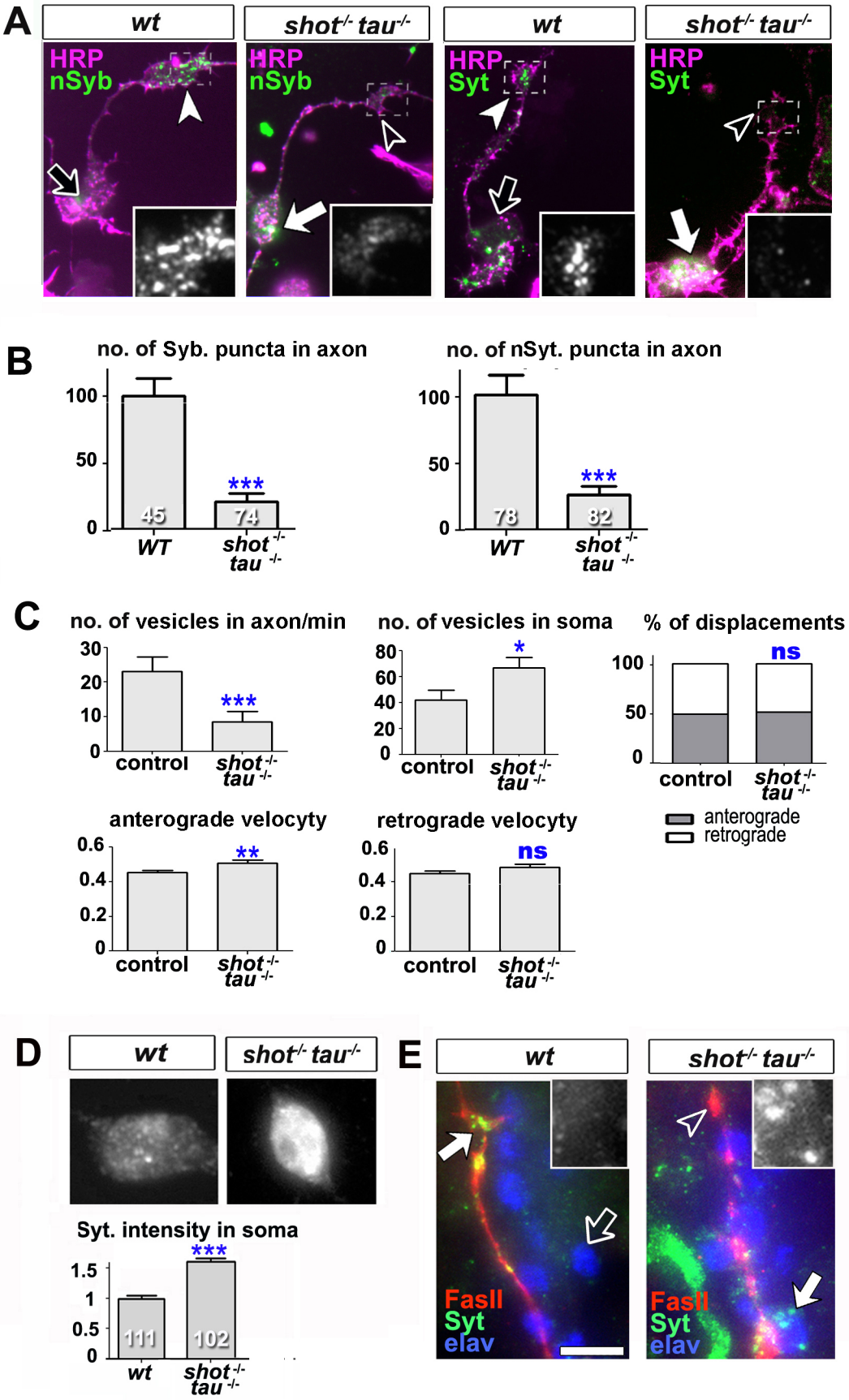
A
wt
shot-/- tau-/-
wt
shot-/- tau-/-
HRP
nSyb
HRP
nSyb
HRP
Syt
HRP
Syt
B
no. of Syb. puncta in axon
100
50
0
***
45
74
WT
shot -/-
tau -/-
no. of nSyt. puncta in axon
100
50
0
***
78
82
WT
shot -/-
tau -/-
C
no. of vesicles in axon/min
30
20
10
0
***
control
shot -/-
tau -/-
no. of vesicles in soma
80
60
40
20
0
*
control
shot -/-
tau -/-
% of displacements
100
50
0
ns
control
shot -/-
tau -/-
anterograde
retrograde
anterograde velocyty
0.6
0.4
0.2
0
**
control
shot -/-
tau -/-
retrograde velocyty
0.6
0.4
0.2
0
ns
control
shot -/-
tau -/-
D
wt
shot-/- tau-/-
Syt. intensity in soma
1.5
1
0.5
0
***
111
102
wt
shot -/-
tau -/-
E
wt
shot-/- tau-/-
FasII
Syt
elav
FasII
Syt
elav

Fig-5

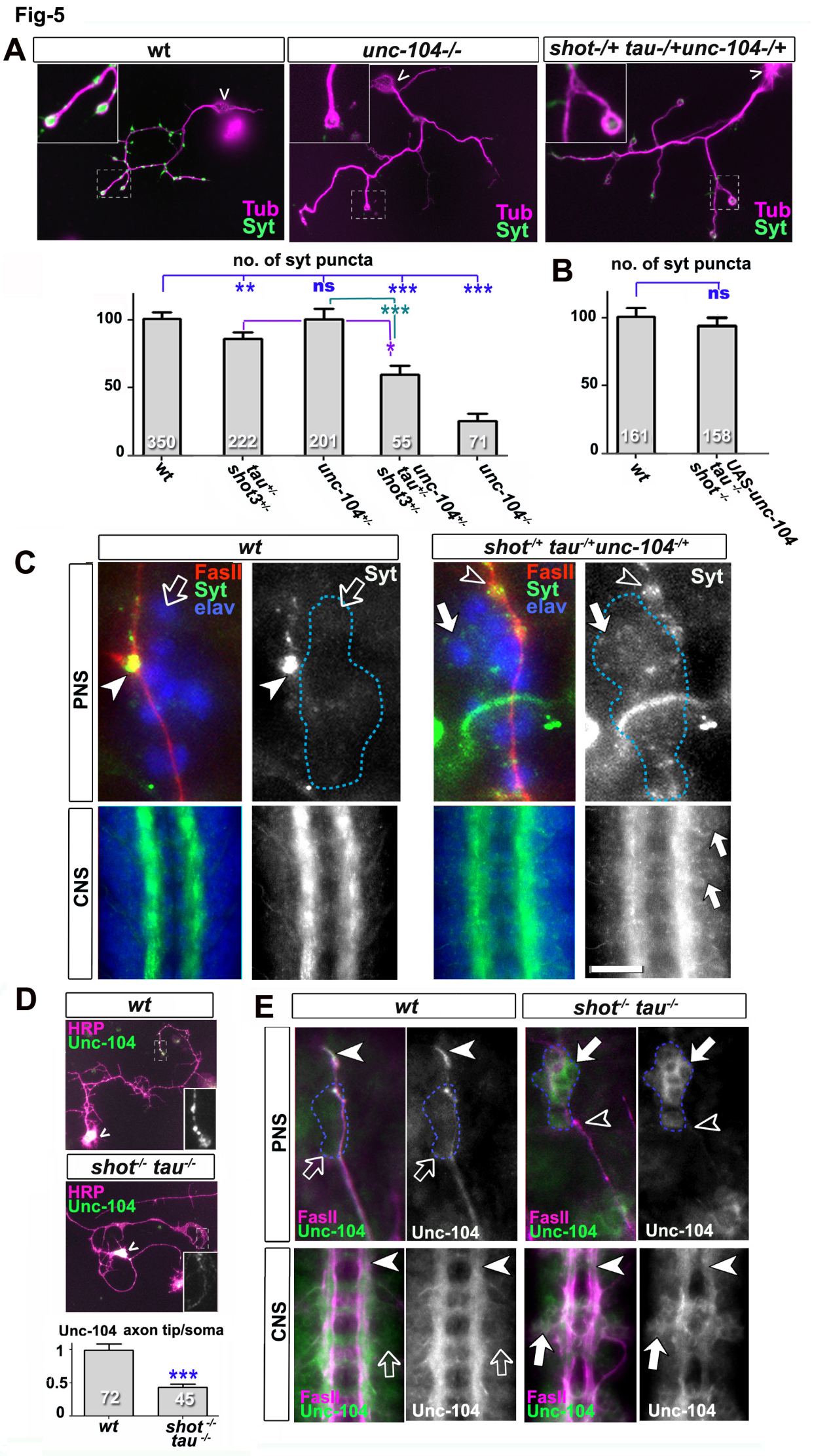
A
wt
unc-104-/-
shot-/+ tau-/+unc-104-/+
Tub
Syt
no. of syt puncta
**
ns
***
***
***
*
100
50
0
350
222
201
55
71
wt
tau+/- shot3+/-
unc-104+/-
unc-104+/- tau+/- shot3+/-
unc-104-/-
B
no. of syt puncta
ns
100
50
0
161
158
wt
tau-/- shot-/-
UAS-unc-104
C
wt
shot-/+ tau-/+unc-104-/+
PNS
CNS
FasII
Syt
elav
D
wt
shot-/- tau-/-
HRP
Unc-104
Unc-104 axon tip/soma
1
0.5
0
***
72
45
wt
shot -/- tau -/-
E
wt
shot-/- tau-/-
PNS
CNS
FasII
Unc-104

Fig-5S1

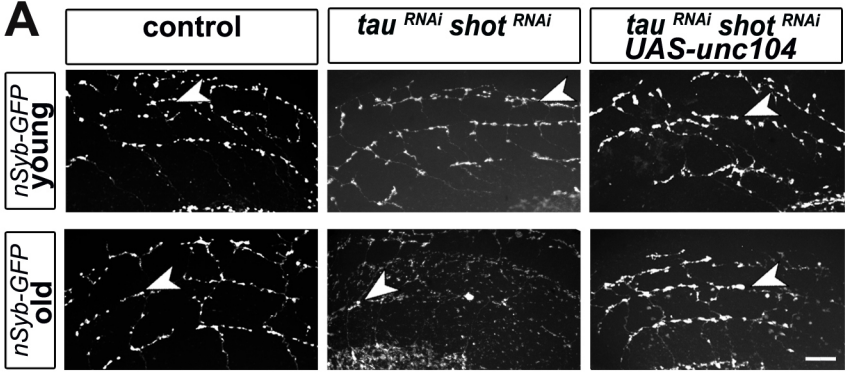
A
control
tau RNAi shot RNAi
tau RNAi shot RNAi
UAS-unc104
nSyb-GFP
young
nSyb-GFP
old

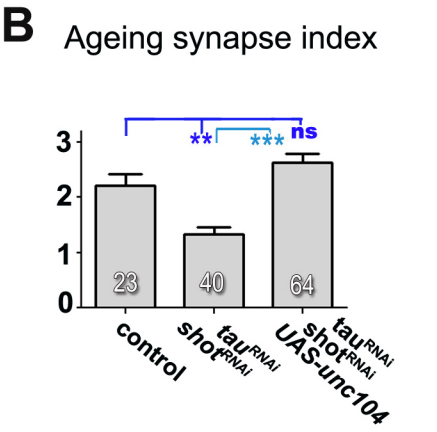
B
Ageing synapse index
**
***
ns
3
2
1
0
23
40
64
control
tauRNAi shotRNAi
tauRNAi shotRNAi UAS-unc104

Fig-6

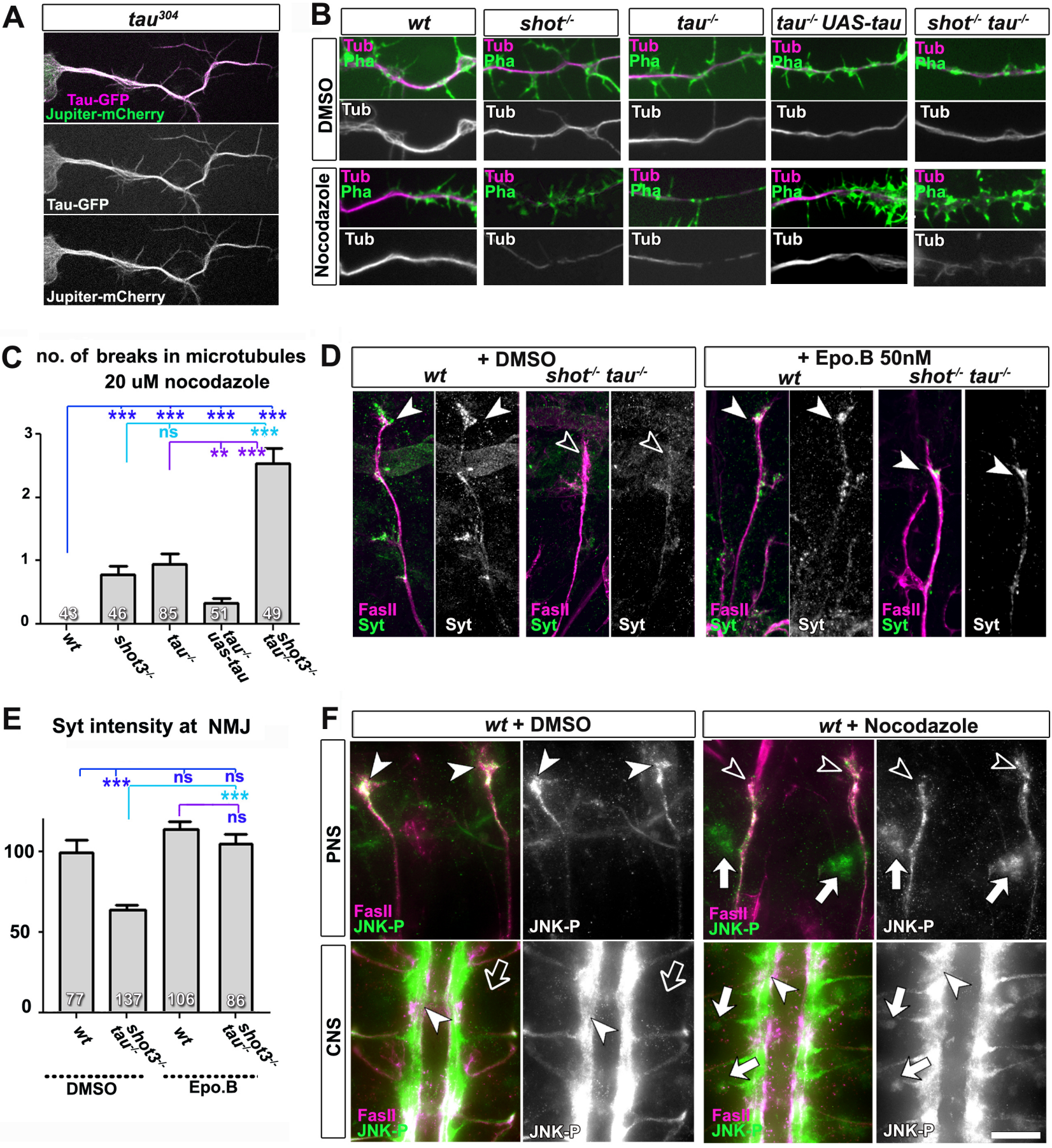
A
tau304
Tau-GFP
Jupiter-mCherry
Tau-GFP
Jupiter-mCherry
B
wt
shot-/-
tau-/-
tau-/- UAS-tau
shot-/- tau-/-
DMSO
Nocodazole
Tub
Pha
Tub
C
no. of breaks in microtubules
20 uM nocodazole
***
ns
**
43
46
85
51
49
wt
shot3-/-
tau-/-
tau-/- uas-tau
shot3-/- tau-/-
D
+ DMSO
+ Epo.B 50nM
wt
shot-/- tau-/-
FasII
Syt
E
Syt intensity at NMJ
ns
77
137
106
86
DMSO
Epo.B
F
wt + DMSO
wt + Nocodazole
PNS
CNS
FasII
JNK-P

Fig-6 S1

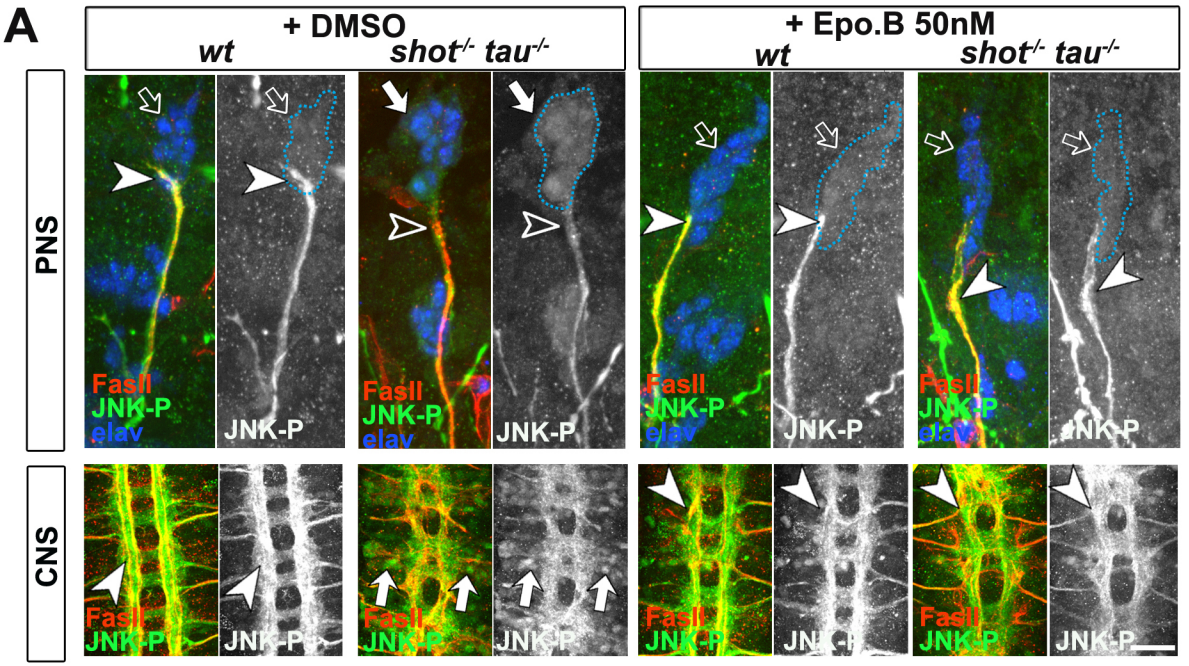
A
+ DMSO
wt
shot-/- tau-/-
+ Epo.B 50nM
wt
shot-/- tau-/-
PNS
CNS
FasII
JNK-P
elav
JNK-P

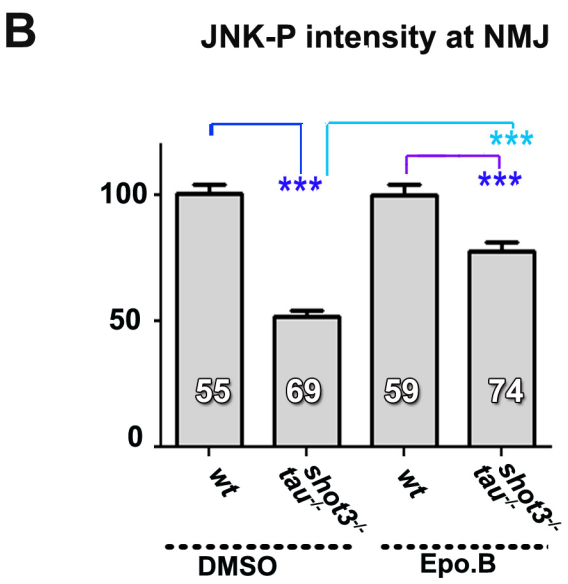
B
JNK-P intensity at NMJ
***
***
***
100
50
0
55
69
59
74
wt
shot3-/-
tau-/-
wt
shot3-/-
tau-/-
DMSO
Epo.B

Fig-7

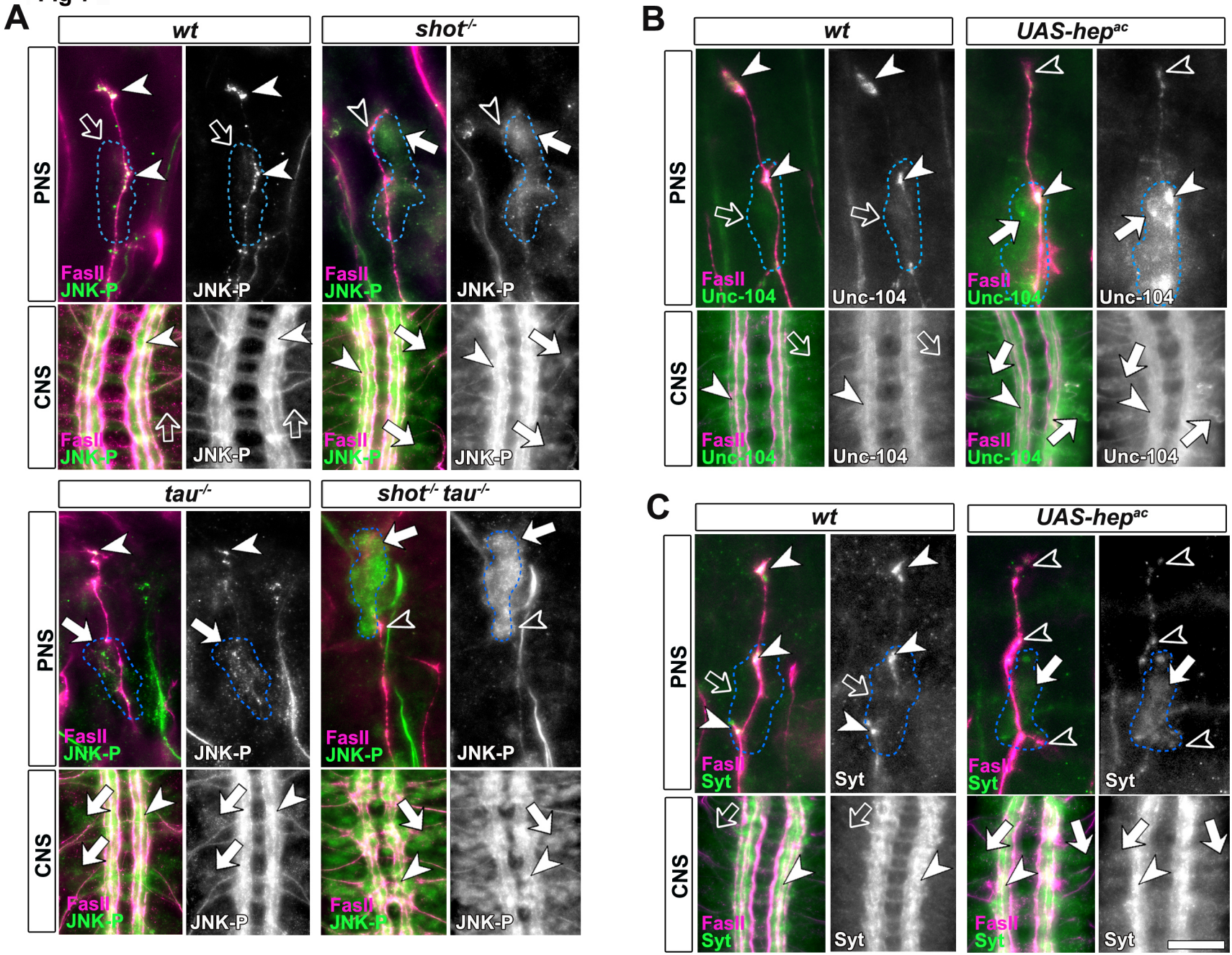
A
wt
shot-/-
tau-/-
shot-/- tau-/-
PNS
CNS
FasII
JNK-P
B
wt
UAS-hepac
Unc-104
C
Syt

Fig-8

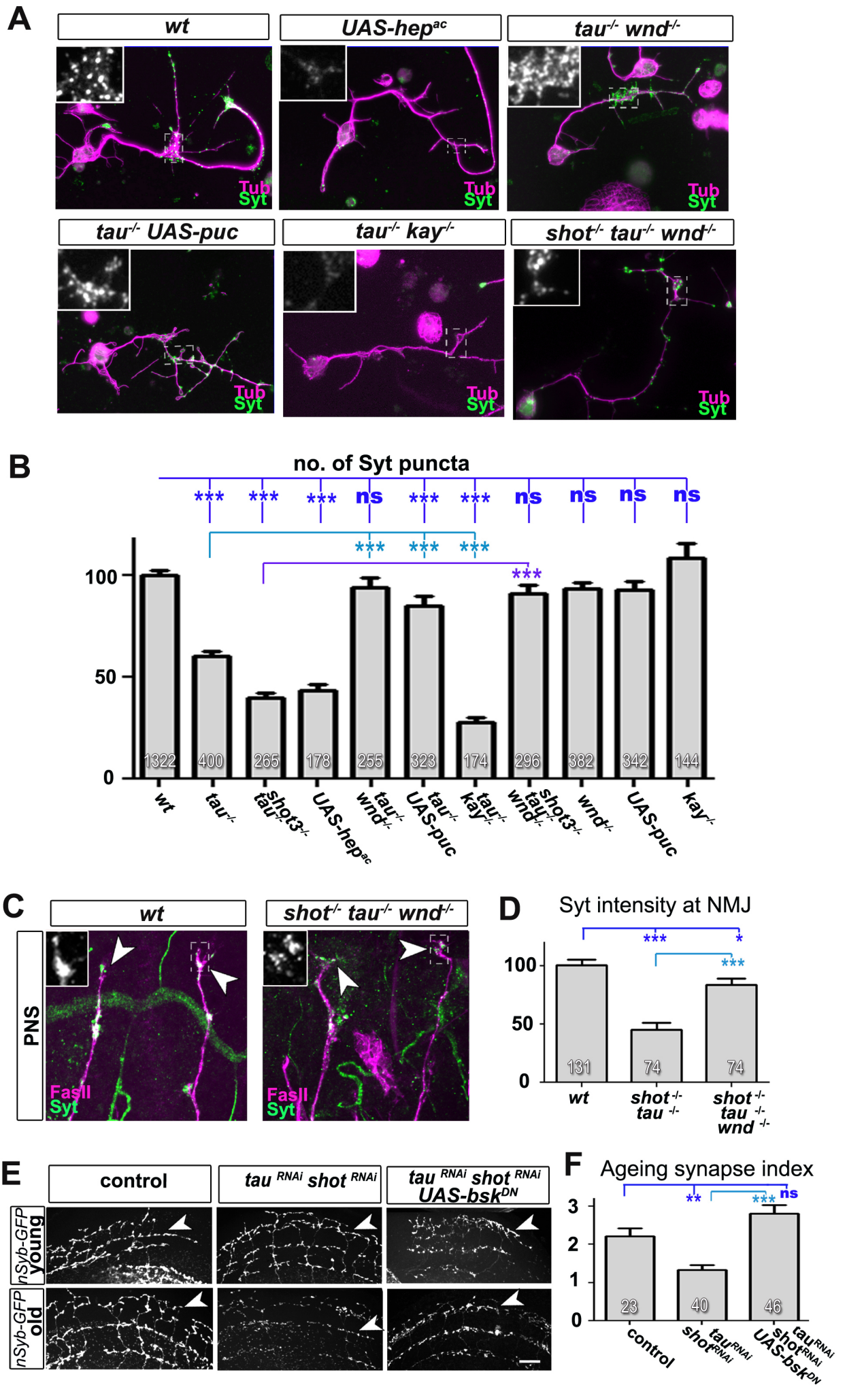
A
wt
UAS-hepac
tau-/- wnd-/-
tau-/- UAS-puc
tau-/- kay-/-
shot-/- tau-/- wnd-/-
Tub
Syt
B
no. of Syt puncta
***
ns
100
50
0
1322
400
265
178
255
323
174
296
382
342
144
wt
tau-/-
shot3-/- tau-/-
UAS-hepac
tau-/- wnd-/-
tau-/- UAS-puc
tau-/- kay-/-
shot3-/- tau-/- wnd-/-
wnd-/-
UAS-puc
kay-/-
C
wt
shot-/- tau-/- wnd-/-
PNS
FasII
Syt
D
Syt intensity at NMJ
*
100
50
0
131
74
74
wt
shot-/- tau-/-
shot-/- tau-/- wnd-/-
E
control
tau RNAi shot RNAi
tau RNAi shot RNAi UAS-bskDN
nSyb-GFP young
nSyb-GFP old
F
Ageing synapse index
**
3
2
1
0
23
40
46
control
tauRNAi shotRNAi
tauRNAi shotRNAi UAS-bskDN

Fig-8 S1

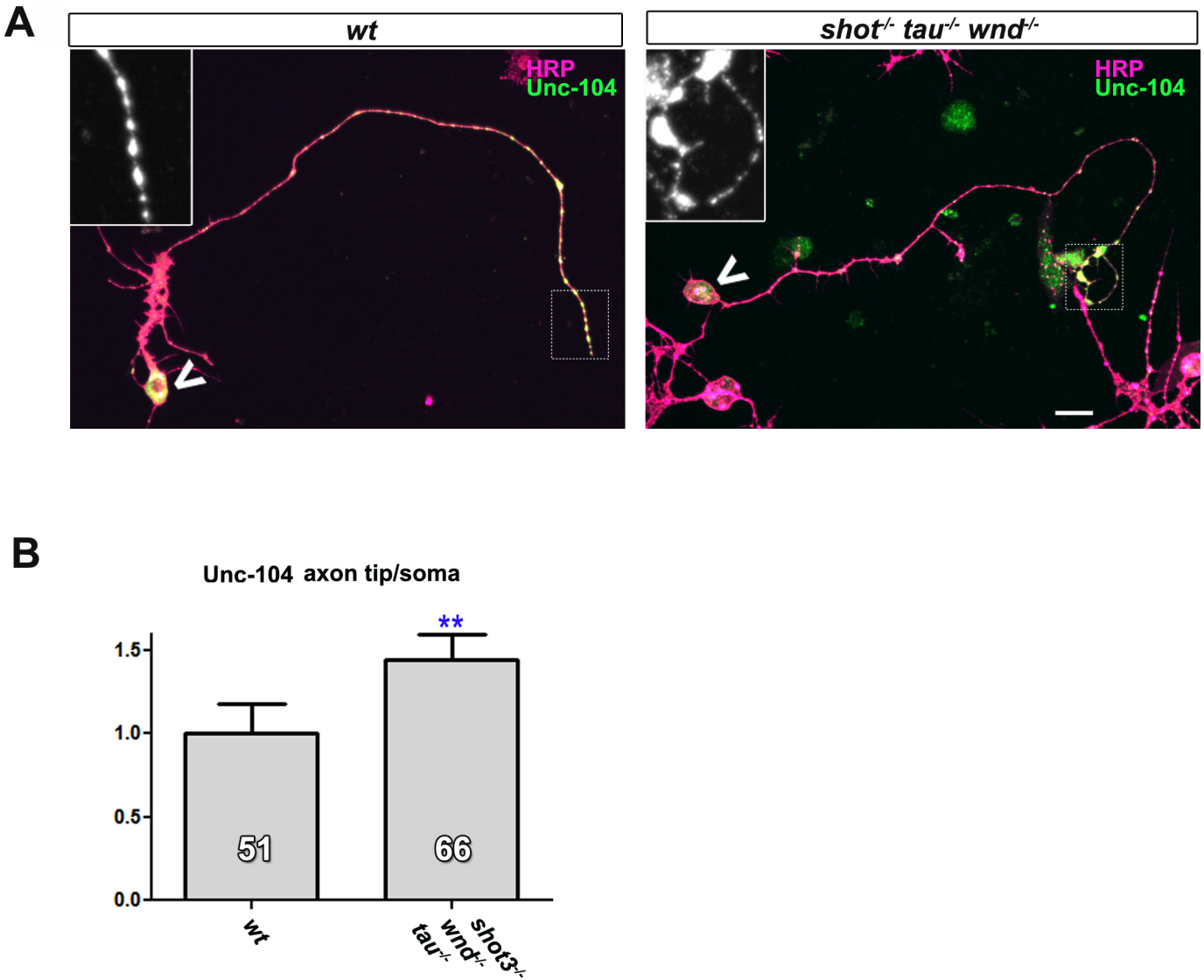
A
wt
HRP
Unc-104
shot-/- tau-/- wnd-/-
HRP
Unc-104
B
Unc-104 axon tip/soma
**
1.5
1.0
0.5
0.0
51
66
wt
tau-/- wnd-/- shot3-/-

Fig-8 S2

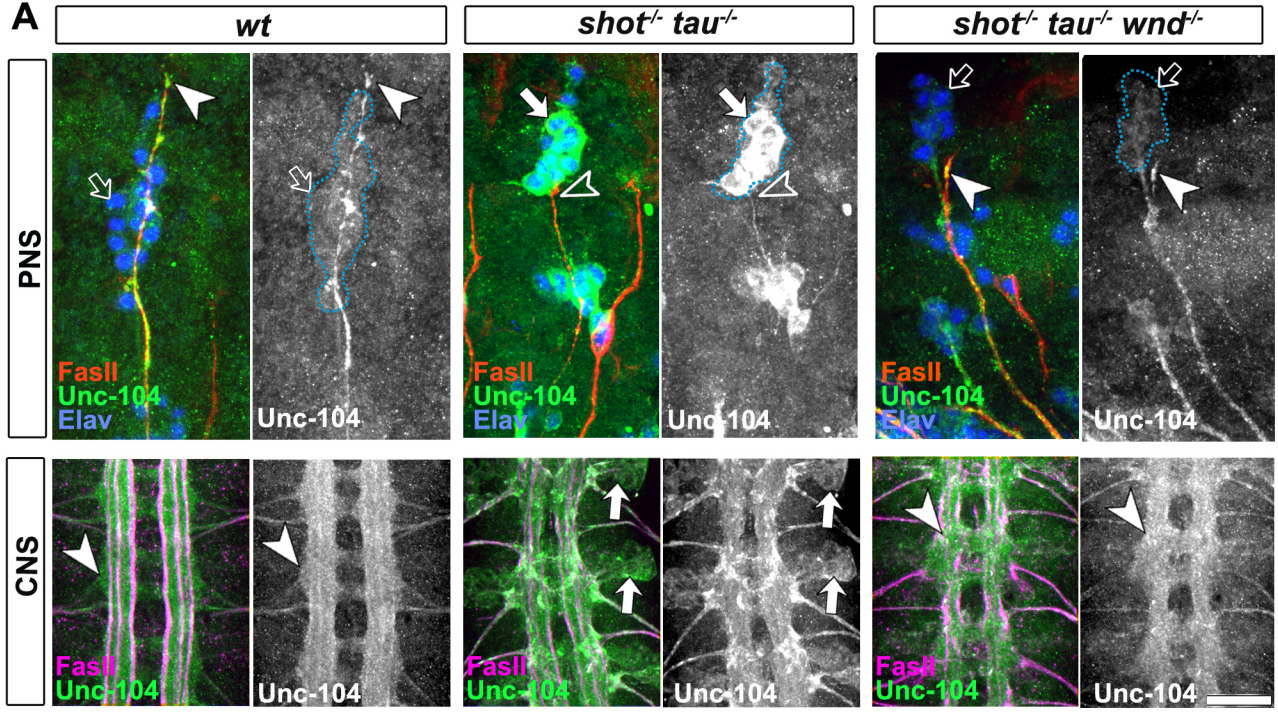

Fig-9

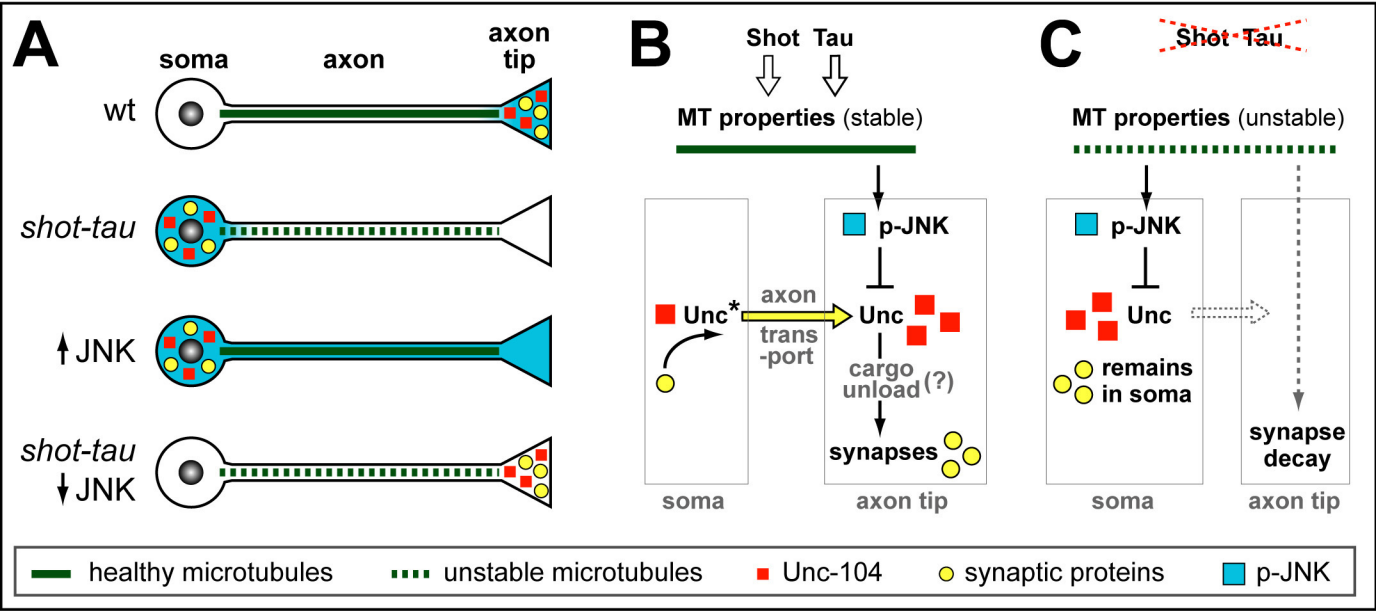
A
soma
axon
axon tip
wt
shot-tau
JNK
shot-tau
JNK
B
Shot Tau
MT properties (stable)
p-JNK
Unc*
axon
trans
-port
Unc
cargo
unload (?)
synapses
soma
axon tip
C
Shot Tau
MT properties (unstable)
p-JNK
Unc
remains
in soma
synapse
decay
soma
axon tip
healthy microtubules
unstable microtubules
Unc-104
synaptic proteins
p-JNK